


Evidence from Tinsihmet Cave in Israel suggests behavioural uniformity across *Homo* groups in the Levantine mid-Middle Palaeolithic circa 130,000–80,000 years ago

Received: 9 September 2023

Accepted: 6 January 2025

Published online: 11 March 2025

 Check for updates

Yossi Zaidner¹✉, Marion Prévost¹, Ruth Shahack-Gross², Lior Weissbrod³, Reuven Yeshurun⁴, Naomi Porat⁵, Gilles Guérin⁶, Norbert Mercier⁷, Asmodée Galy^{7,8}, Christophe Péchevran⁸, Gaëlle Barbotin⁸, Chantal Tribolo⁷, Hélène Valladas⁶, Dustin White⁹, Rhys Timms⁹, Simon Blockley⁹, Amos Frumkin¹⁰, David Gaitero-Santos¹, Shimon Ilani⁵, Sapir Ben-Haim¹, Antonella Pedergnana¹¹, Alyssa V. Pietraszek¹², Pedro García^{12,13}, Cristiano Nicosia¹³, Susan Lagle⁴, Oz Varoner¹⁴, Chen Zeigen^{1,15}, Dafna Langgut^{16,17}, Onn Crouvi⁵, Sarah Borgel^{18,19}, Rachel Sarig^{19,20}, Hila May^{18,19} & Israel Hershkovitz^{18,19}

The south Levantine mid-Middle Palaeolithic (mid-MP; ~130–80 thousand years ago (ka)) is remarkable for its exceptional evidence of human morphological variability, with contemporaneous fossils of *Homo sapiens* and Neanderthal-like hominins. Yet, it remains unclear whether these hominins adhered to discrete behavioural sets or whether regional-scale intergroup interactions could have homogenized mid-MP behaviour. Here we report on our discoveries at Tinsihmet Cave, Israel. The site yielded articulated *Homo* remains in association with rich assemblages of ochre, fauna and stone tools dated to ~100 ka. Viewed from the perspective of other key regional sites of this period, our findings indicate consolidation of a uniform behavioural set in the Levantine mid-MP, consisting of similar lithic technology, an increased reliance on large-game hunting and a range of socially elaborated behaviours, comprising intentional human burial and the use of ochre in burial contexts. We suggest that the development of this behavioural uniformity is due to intensified inter-population interactions and admixture between *Homo* groups ~130–80 ka.

Studies on the mid-Middle Palaeolithic (mid-MP; ~130–80 thousand years ago (ka)) document an increased pace of out-of-Africa hominin dispersals and provide a growing body of evidence that southwest Asia was the stepping stone for an Asia-wide expansion of *Homo sapiens*^{1,2}. The Levant during this period is marked by exceptional evidence of synchronous human morphological variability within the region, including fossil evidence of highly variable populations^{3–6}. This variability is expressed on the inter-site level

with archaic Neanderthal-like fossils reported at Nesher Ramla⁵ and *H. sapiens*-like fossils at Skhul and Qafzeh caves^{3,4,7}, between the Skhul and Qafzeh fossils^{8–11}, and on the intra-site level within the Qafzeh human fossil assemblage^{6–8,11–14}. This variability has been a source of major debate about the anatomical affinities of Levantine mid-MP hominins. Skhul and Qafzeh hominins have been variously seen as variable populations of archaic *H. sapiens*^{7,15–17}, distinct human types or hybrids^{3,8,11,13,18,19}.

A full list of affiliations appears at the end of the paper. ✉e-mail: yzaider@mail.huji.ac.il

High human morphological diversity in the Levantine mid-MP is accompanied by abundant evidence of complex social behaviour such as intentional burial of the dead, the interment of grave goods and ochre use in burial sites^{3,4,20–24}, which predates all other such evidence in the global record by tens of thousands of years. At present, the Levantine mid-MP behavioural evidence is unevenly spread across sites, resulting in long-lingering uncertainties in interpreting regional variability in material culture and its behavioural implications.

The four key Levantine sites that include human-fossil-bearing deposits and are broadly assigned to the mid-MP—namely, Qafzeh, Skhul, Tabun and Nesher Ramla—are currently characterized by a lack of coherence. To date, the most complete package of material markers of technological and symbolic human behaviours derives from Qafzeh Cave. Excavations in this site have uncovered seven burials^{4,21}, associated with grave goods and abundant ochre pieces^{22,23}, and large lithic assemblages that demonstrate the technological dominance of the centripetal Levallois method²⁵. This knapping technology is considered a defining characteristic of mid-MP lithic technology in southwest Asia^{5,25–30}.

The assignment of two other mid-MP-affiliated sites, Skhul and Tabun Layer C, to a mid-MP stage of cultural development has long been a matter of debate^{25,26,28,31–36}, which has drawn on a range of considerations from material culture, chronology and human anatomical remains. The affiliation of Skhul and Tabun Layers B and C lithic assemblages with those of Qafzeh remains uncertain due to their small size, non-systematic early twentieth-century collection methods and inconsistency in the dating results. Various authors continue to argue for the absence of chronological overlap among these mid-MP-associated strata^{37–42}.

Additionally, the recently uncovered, large lithic assemblage of Nesher Ramla reveals that the Levallois centripetal reduction system was the primary technology employed at this site^{28,29,43}. While mid-MP Nesher Ramla may closely align with Skhul and Qafzeh chronologically²⁹, its human fossils belong to a palaeodeme associated with archaic Neanderthal-like hominins⁵. The south Levantine mid-MP thus represents a pivotal testing ground for issues involving the technological, symbolic, anatomical and genetic repercussions of local population admixture processes.

Here we report on the recent discoveries at Tinsmet Cave, Israel, which is located only 10 km from the open-air site of Nesher Ramla. We systematically evaluate the likelihood that these sites, together with Qafzeh, Skhul and Tabun C, belonged to a coherent regional cultural tradition widely shared among hominin groups of diverse anatomical affiliations. Tinsmet Cave has yielded large lithic assemblages dominated by centripetal Levallois technology associated with numerous *Homo* spp. remains, including fully articulated skeletons, and abundant ochre chunks. Excavations at the cave put into perspective the question of lithic regional technological variability, shedding light on the unifying role of the centripetal Levallois reduction system across the mid-MP southern Levant and revealing the widespread occurrence of a novel repertoire of complex social behaviours. This study reveals tight connections between mid-MP lithic technological behaviour and the local development and elaboration of social and symbolic behaviours within one coherent and uniform cultural complex.

Site formation, stratigraphy and chronology

Tinsmet Cave (Mugharet Al Watwat⁴⁴) is situated on the east bank of Nahal Beit Arif in central Israel (Fig. 1 and Extended Data Fig. 1)⁴⁵. The cave is composed of a Terrace and three chambers, with the deepest one now featuring an open chimney (Fig. 1 and Supplementary Section 1). Preliminary inspection of the cave by M. Stekelis in 1940 documented the presence of Middle and Upper Palaeolithic lithic artefacts⁴⁴. Our excavations revealed that MP deposits extend across much of the exterior Terrace and the First Chamber of the cave, whereas the second and third chambers of the cave lack evidence of human occupation.

The main activity area of the site was the Terrace, which was probably partially roofed during the human occupation. The Terrace consists of 2–2.5-m-thick cemented sediments composed of varying amounts of calcite, clays and quartz, with the first originating mainly from wood ash, fragments of the cave wall and secondary calcite. The clays originate primarily from reworked terra rossa soil above the cave; the quartz grains are of aeolian origin, most likely from the active dunes along the coastal plain to the west^{46,47} (Supplementary Sections 2 and 3). The sediments also contain carbonated hydroxylapatite that primarily originates from bones, carnivore coprolites and meagre authigenic phosphate nodules. The deposits were divided into three units—A, B and C (Figs. 1 and 2), with Unit A further subdivided into five layers (A1–A5) and Unit B into two layers (B1a and B1b) on the basis of differences in the density of the archaeological remains and the presence/absence of rock fragments that have collapsed from the cave ceiling and walls (Supplementary Section 2).

The sedimentological sequence begins with the archaeologically poor Unit C. This unit includes a small number of lithic artefacts, carnivore coprolites and no traces of wood ash, and it is likely to represent either ephemeral or no human occupation. Unit C rests on a phosphatized limestone bedrock, indicating the degradation of bat guano and carnivore coprolites—that is, a roofed cave environment. According to absolute dates, the sediments of Unit C accumulated at a slow rate (Fig. 2). Well-preserved pollen uncovered in Unit C indicates a Mediterranean open forest with fairly wide-spaced trees, small shrubs and herbs dominated by evergreen oak (Supplementary Section 4). In contrast, the overlying Units A and B of the Terrace deposits show evidence of intensive human occupation, with the sediments consisting of recrystallized wood ash and an accumulation of other fire residues such as microcharcoal, carbonized and calcined bone fragments, and ash pseudomorphs (Extended Data Fig. 2 and Supplementary Section 3). Unit A includes more secondary calcite and is more indurated than Unit B. Cementation of the remains of combustion activities probably occurred by water percolation downwards and along cracks, where secondary calcite can be detected. The sediments are bioturbated (primarily insect and plant rooturbation). Therefore, clear combustion features (such as hearths) were not detected. The intensive use of fire at the site is also evident from the high frequencies of burnt lithics.

Within the cave, the First Chamber is divided into inner and outer parts. The outer part of this chamber, located near the present-day dripline, is composed of anthropogenic sediments similar to those found on the Terrace, albeit less cemented. The sedimentological sequence of the First Chamber is about 1 m thick down to the bedrock (Fig. 1 and Supplementary Section 2), and the bulk of the deposits are assigned to Layer III (Fig. 1). Layer III shows mineralogical composition similar to that of Unit A on the Terrace and is likely to represent the same stratigraphic unit⁴⁶ (Supplementary Section 3).

The inner part of the chamber contains a soft, dark brown, non-anthropogenic accumulation composed primarily of clay and quartz (Dark Brown (DB) Layer). This layer consists of reworked terra rossa soil that infiltrated the cave from its interior chimney and entrance (Figs. 1 and 2 and Supplementary Sections 2 and 3). The DB Layer contains some artefacts, which were probably redeposited from in situ deposits in the outer part of the First Chamber.

Thermoluminescence dating

The thermoluminescence (TL) dating method applied to burnt flints from Layer III in the First Chamber provides ages with relatively low dispersion, ranging from 84 to 109 ka, with a mean age of 96.3 ± 7.2 ka (Fig. 2, Extended Data Table 1 and Supplementary Section 5). Burnt flints from the Terrace demonstrate a much higher dispersion of ages than the cave deposits, mainly because of two samples from Unit B1b, which give ages of 173 ± 20 and 153.8 ± 12 ka, and two samples from Unit C, which give ages of 124 ± 14 and 117 ± 14 ka (mean age, 120.4 ± 14 ka). These four samples indicate that the bottom of Unit B1b and Unit C may

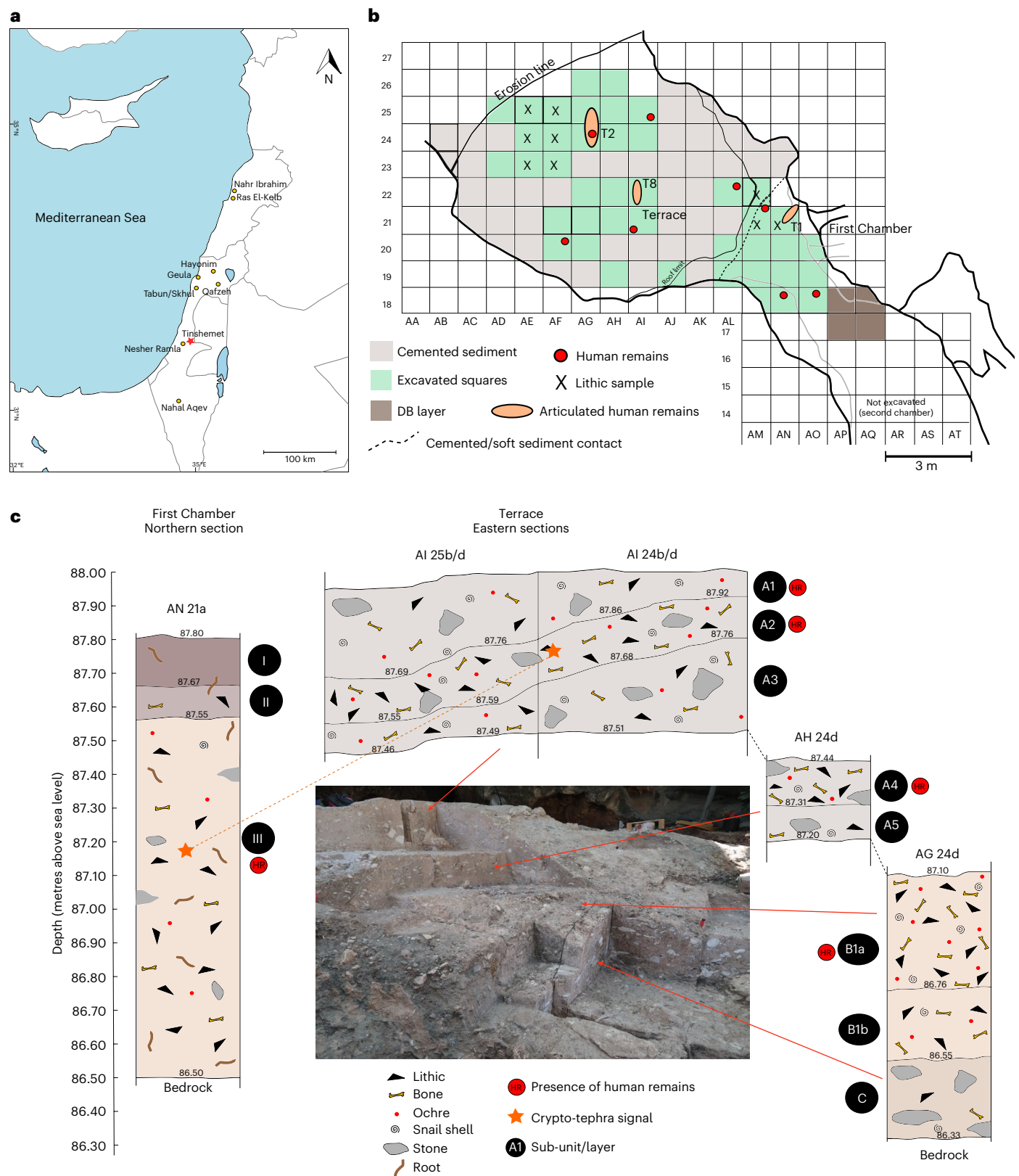


Fig. 1 | Tinshemet Cave, geographical location, cave plan and stratigraphy. a, Location of Tinshemet Cave and other major mid-MP sites in the Levant. **b,** Plan of the Terrace and the First Chamber of the cave. **c,** Stratigraphic sections of the outer part of the First Chamber and the Terrace, and field image of the Terrace

sediments. The red circles denote articulated human remains. The orange stars connected by a dashed line denote the locations of volcanic shards with similarly evolved rhyolitic signatures that suggest a chronological correlation between Unit A on the Terrace and Layer III in the outer part of the Inner Chamber.

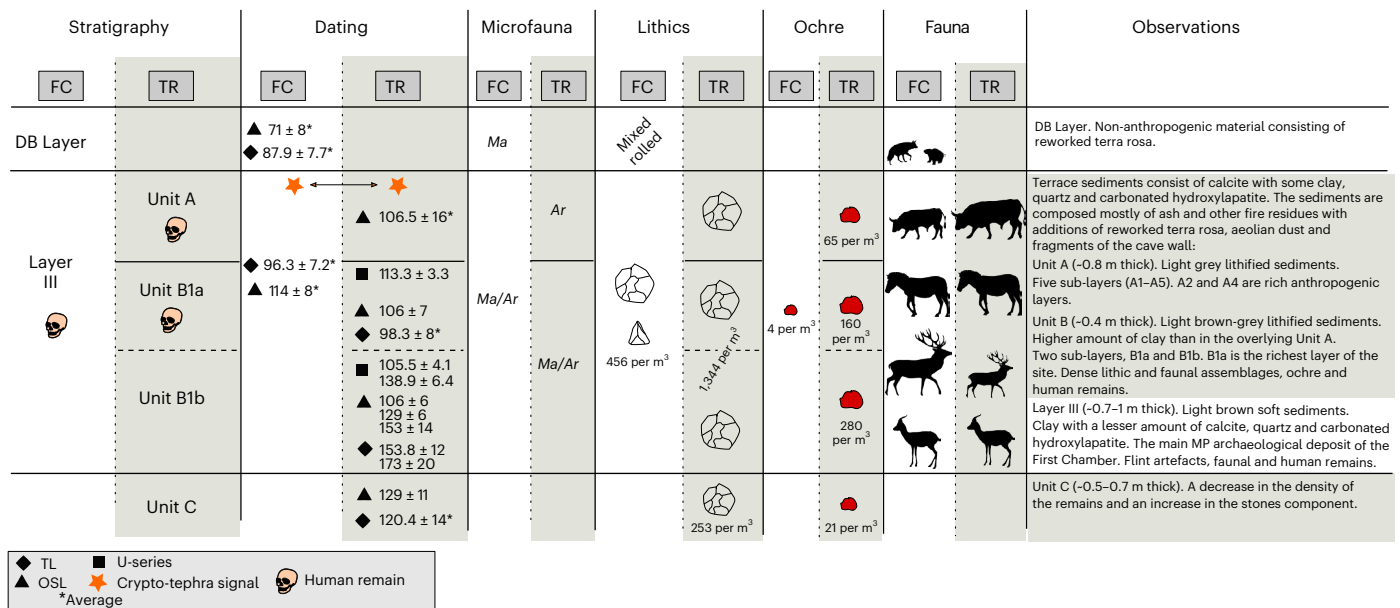


Fig. 2 | Tinsihmet Cave: major characteristics. Archaeological and environmental characteristics (stratigraphy, dating, microfauna, lithics, ochre and fauna) of the Terrace and the First Chamber. Ages are given in ka. When mean ages are presented, they are marked with an asterisk. FC, First Chamber; TR, Terrace; Ar, *Arvicanthis*; Ma, *Mastomys*. Smaller icons for lithics and ochre

indicate smaller ratios. Smaller animal icons indicate their lower frequencies in the assemblages. Credit: Silhouettes from PhyloPic under a Creative Commons license [CC0 1.0](https://creativecommons.org/licenses/by/4.0/): porcupine, T. Michael Keesey; hyena, Margot Michaud; horse, Lisa Nicvert; deer, Feeran Sayol; aurochs, Mariana Ruiz Vilarreal. Skull icon by purzen adapted from OpenClipArt under a Creative Commons license [CC0 1.0](https://creativecommons.org/licenses/by/4.0/).

represent an earlier human presence at the site. Apart from these four samples, the remaining six TL samples from the Terrace yielded a mean age of 98.3 ± 8.0 ka, which is indistinguishable from the mean value obtained for the flints from the First Chamber (Extended Data Fig. 3). The burnt flints from the non-anthropogenic DB Layer in the inner part of the First Chamber (1, 22 and 14-1) probably represent reworked material and provide a mean age of 87.9 ± 7.7 ka.

Optically stimulated luminescence dating

Optically stimulated luminescence (OSL) ages were obtained from quartz grains extracted from the sediments. The OSL ages for the Terrace Unit A layers yielded a mean age of 106.5 ± 16 ka (Fig. 2, Extended Data Table 2 and Supplementary Section 6). A single age from Unit B1a is 106 ± 7 ka, while the ages from Unit B1b show a high dispersion with ages of 106 ± 6 , 129 ± 6 and 153 ± 14 ka. A single sample from Unit C yielded an age of 129 ± 11 ka. The OSL age for Layer III in the First Chamber is 114 ± 8 ka. The DB Layer provided an average age of 71 ± 8 ka, suggesting that these sediments accumulated after human use of the cave had ceased.

Uranium-series dating with laser-ablation inductively coupled plasma mass spectrometry

Images of radioisotopes relevant for uranium-series (U-series) dating were produced using a laser ablation (LA) module and a high-resolution inductively coupled plasma (ICP) mass spectrometry (MS) system. Two types of samples were dated: veins of secondary calcite and snail shells. Two samples were taken from thin calcite veins deposited in fissures formed in the cemented deposits of Unit A on the Terrace. The isochron ages computed using the Java code⁴⁸ are 15.6 ± 0.2 ka and 35.6 ± 1.1 ka. These ages suggest that the infilling of the fissures with calcite is a relatively recent Late Pleistocene phenomenon (Supplementary Section 7). Snail shells taken from Unit B revealed U values distributed according to the growth layers of the shells⁴⁹, with the variability ranging from a few ppb up to 200–300 ppb (Supplementary Section 7). The ^{232}Th content is very low and homogeneous inside the shell, indicating that it was incorporated during growth. Three samples provide ages (113.3 ± 3.3 / -3.5 ka, 105.5 ± 4.1 ka and 138.9 ± 6.4 / -6.0 ka) that are

in agreement with the TL and OSL age distributions (Fig. 2, Extended Data Fig. 3 and Extended Data Table 3). A fourth shell gives an older age (>272 ka), with higher uncertainties mainly related to the asymptotic nature of the growth curve of the $^{230}\text{Th}/^{234}\text{U}$ activity ratio.

Cryptotephra

The results of the cryptotephra (microscopic volcanic ash) analysis show low shard abundance both on the Terrace and in the First Chamber (Supplementary Section 8). Compositional data were successfully obtained from three glass shards, one representing Unit A on the Terrace and two representing Layer III in the First Chamber. The shard from Unit A and one of the shards from Layer III exhibit evolved rhyolitic signatures that are similar enough to suggest a correlation between Unit A on the Terrace and Layer III in the First Chamber. The measured samples also exhibit a glass chemical signature similar to volcanoes from the Aegean Arc, such as Kos, as well as eruption centres in Central Anatolia (for example, Acigöl⁵⁰). The Tinsihmet Cave shards show a good level of similarity to the recently published tephra from the Marine Isotope Stage (MIS) 5 Nahal Aqev site, Israel³⁴ (Supplementary Section 8).

The micromammals

Altogether, eight taxa were identified (Supplementary Section 9). Most of these taxa typically occur in mid-late Pleistocene fossil assemblages from southwest Asia (Supplementary Section 9). However, two of the taxa (*Mastomys batei* and *Arvicanthis ectos*) represent key index fossil species (that is, *fossiles directeurs*) of the regional biostratigraphy, which alternately occupied the region during different stages of the MP³³ and were last documented within this region during MIS 5 (ref. 51). The presence of these two taxa, together with their relative and rank abundance in the assemblage, identify the Tinsihmet Cave deposits as an analogue of mid-MP Qafzeh Layers XV–XXV. Despite the rather small size of the Tinsihmet Cave assemblage and attendant limitations for quantitative analysis, the observation that one tooth of either *Mastomys* or *Arvicanthis* was uncovered for every 18 specimens of all other rodent taxa (a 1:18 ratio) suggests temporal affiliation with Qafzeh. The equivalent ratio for all Qafzeh layers combined is 1:20 (ref. 51), while the



Fig. 3 | Lithic artefacts from Tinsmet Cave. **a**, Recurrent centripetal Levallois core. **b**, Centripetal Levallois core. **c**, Preferential Levallois core with centripetal preparation. **d**, Preferential Levallois core. **e**, *Débordant* flake. **f**, *Débordant* and *outrépassé* flake. **g**, *Éclat débordant à dos limité* (pseudo-Levallois flake). **h**, *Éclat débordant à dos limité* (pseudo-Levallois flake). **i**, *Éclat débordant à dos limité*

(pseudo-Levallois flake). **j**, Centripetal Levallois flake. **k**, Centripetal Levallois flake. **l**, Levallois flake with bidirectional scar pattern. **m**, Centripetal Levallois flake. **n**, Levallois flake with bidirectional scar pattern. **o**, Levallois point. **p**, Scraper on centripetal Levallois flake. **q**, Scraper on Levallois flake.



Fig. 4 | Different types of ochre from Tinsihemet Cave and their association with human and animal bones. a, Ochre types. Class I: sandstone, distinguishable sand grain size and crumbly, high abundance of quartz mineral; Class II: fine-grained laminated and compacted clay, with high abundance of quartz mineral and very low to non-existent carbonates; Class III: calcium-carbonated formation and low abundance of quartz grains; Class IV: heterogenic anisotropic grains, unstructured heterogeneous fabric, with anisometric

and contiguous quartz crystals; Class V: oolitic sandstone; Class VI: poorly compacted sandstone. **b,** In situ piece of ochre located between the human leg long bones (Tinsihemet 2). **c,** Ochre piece associated with several fragmented animal bones and lithic artefacts in Unit B1a in square AF23 (same sub-unit and ~1 m from Tinsihemet 2). **d,** Ochre pieces associated with several fragmented animal bones and lithic artefacts in Unit A4 in square AG22.

early-MP deposits of Misliya and Hayonim Layer E show a remarkable difference with ratios of 1:70 and 1:600, respectively^{33,51}.

Summary of the chronostratigraphic results

Dosimetric (TL and OSL) and U/Th dating methods indicate that Tinsihemet Cave was inhabited during the MIS 5 (130–80 ka; Fig. 2 and Extended Data Fig. 3). The major stages of occupation of the cave are represented by Units A and B on the Terrace and Layer III at the front of the First Chamber. The geoarchaeological, geochronological and biochronological evidence suggests that Unit A on the Terrace and Layer III in the outer part of the First Chamber belong to the same stratigraphic unit. They exhibit similar sedimentological characteristics that include a greyish deposit containing abundant clasts of flint, bones and rocks, variably cemented by partial dissolution and recrystallization of wood ash (Extended Data Fig. 2). The only difference is the presence of carnivore coprolites in Layer III, probably due to its position under the roofed part of the cave. According to TL ages, the main phase of human occupation on the Terrace and in the First Chamber of the cave is dated to 97 ± 9 ka (mean age) (Extended Data Table 1). This mean age is in the range of the U-series ages obtained for Unit B and the OSL ages, which are 106.5 ± 16 ka on average for Unit A, 106 ± 7 ka for Unit B1a and 114 ± 8 ka

for Layer III in the First Chamber (Extended Data Tables 2 and 3). These results suggest that the Terrace (Units A and B) and the outer part of the First Chamber (Layers III) were inhabited at roughly the same time. The contemporaneity of the deposition is also supported by the volcanic glass shards that suggest a potential temporal correlation between Unit A on the Terrace and Layer III in the First Chamber.

The occurrence of the African-tropical rodent taxa *Mastomys* and *Arvicanthis* suggests that similarly to Qafzeh Cave, Tinsihemet Cave is likely to represent mid-MP Biozone II of the regional biostratigraphy (130/120–80 ka; Qafzeh Layers XV–XXV³³). Both taxa at Tinsihemet Cave occur within the First Chamber's deposits (Layer III) and in Units A and B of the Terrace, supporting the contemporaneity of the deposits. The lower part of the Terrace sediment sequence, especially Unit C, probably represents an earlier phase of accumulation (late MIS 6/early MIS 5).

The behavioural repertoire of the Tinsihemet Cave hominins

The lithic assemblages

The Tinsihemet Cave excavation yielded abundant lithic material from both the First Chamber and the Terrace. In the framework of this study,

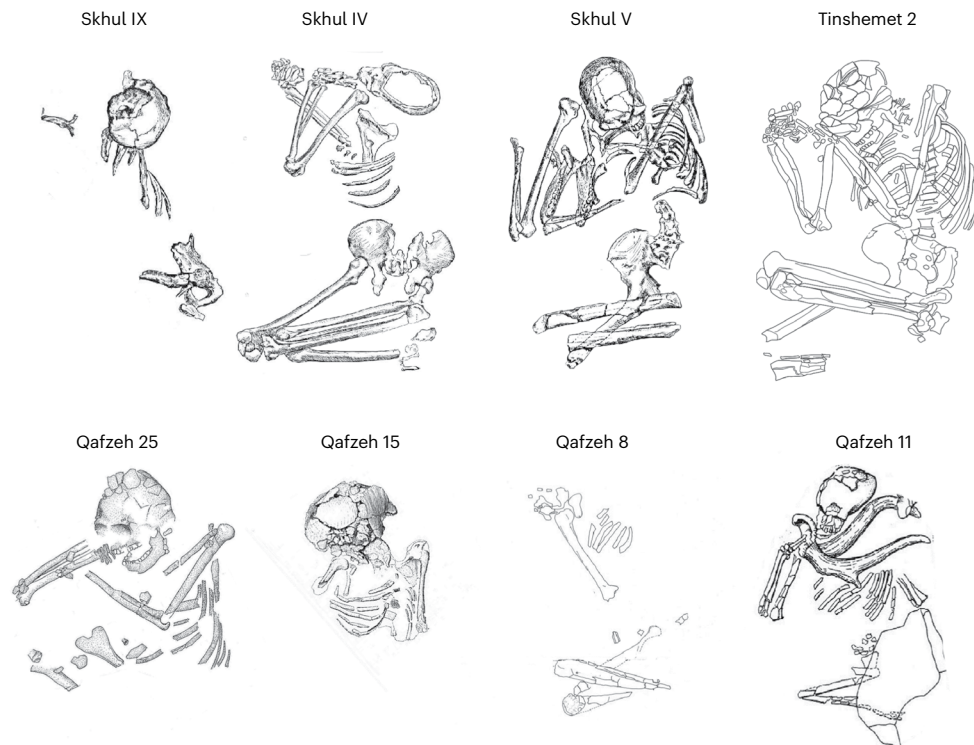


Fig. 5 | Human burials at Tinsihmet, Qafzeh and Skhul Caves. Note that in all three caves the body was deposited on their right side (Qafzeh 9 excluded) in a fetal position, regardless of sex or age. The burials of Skhul IX, IV and V are redrawn from McCown and Keith³, and the burials of Qafzeh 25, 15, 8 and 11 are redrawn from Vandermeersch and Bar-Yosef⁴.

assemblages from Layer III in the First Chamber ($n = 809$) and from Units B and C on the Terrace ($n = 1971$) were studied (Fig. 1 and Extended Data Fig. 4). The results show close technological similarity between these assemblages, suggesting that they are likely to represent the same cultural unit. Local Mishash Formation Campanian flint dominates the assemblages (53% on the Terrace and 70% in the First Chamber; Supplementary Section 10). Flint from indeterminate (non-local) sources forms 15% of the lithic assemblage of the Terrace and 14% of the lithic assemblage of the First Chamber. Thermal alterations were recorded on 44% of artefacts on the Terrace and 36% in the First Chamber. The technology in all excavated areas predominantly comprised flake production by the centripetal Levallois method (Fig. 3 and Extended Data Table 4). Cortical flakes and different types of core trimming elements were identified both on the Terrace and in the First Chamber, suggesting that at least part of the knapping activities took place on-site (Extended Data Fig. 4a).

The centripetal Levallois reduction system is represented by cores and debitage, including both by- and end-products (Fig. 3). Levallois by-products are represented by *débordant* flakes, pseudo-Levallois flakes and points, and striking platform preparation flakes (Fig. 3). Typical Levantine MP lithic components such as Kombewa flakes and core-on-flakes were identified in the assemblages. While Levallois points are exceptionally rare on the Terrace (1%), their frequency is slightly higher in the First Chamber (5%). The frequency of retouched tools is very low: 1.3% on the Terrace and 3.1% in the First Chamber (Fig. 3). The assemblage from the First Chamber shows a minor dominance of single sidescrapers (Extended Data Fig. 4b). In addition, two ‘bulb retouchers’ were identified, one in each of the assemblages. Use-wear analysis identified evidence of use on 19 of the 44 tools examined (Supplementary Section 11). A wide variety of activities were documented, including whittling, scraping, cutting/sawing and perforating bones; whittling and scraping wood; and butchering (Supplementary Section 11).

Ochre

The excavations at Tinsihmet Cave yielded more than 7,500 ochre fragments of different sizes, shapes, textures and colours (Fig. 4 and Supplementary Section 12). There is a clear dominance of red to orange hues (75.7%), followed by brown (16.7%), yellow (5%) and purple hues (2.6%). Some of the exploited pieces have a combination of lighter to darker red tonalities that suggest heating. The density of ochre pieces larger than 5 mm per excavated volume of sediment increases notably from Unit C to Unit A (Fig. 2), with the highest densities recorded in the layers with human burials (Units A and B). Ochre fragments were often found close to the burials, as in the case of a 4–5 cm large chunk of red ochre found between the legs of the Tinsihmet 2 individual (Fig. 4b).

Six different classes of ochre (I to VI) have been identified on the basis of the grain size, grain morphology, and the presence/absence and size of quartz crystals (Fig. 4 and Supplementary Section 12). The characteristics of the ochre allow us to infer at least four different sources including sandstones (with closest available source as far as the Galilee in the north, at least 60–80 km from the site), limestone and iron-rich formations possibly as far as the central Negev (>100 km to the south). The exploitation of distant sources suggests that great efforts were invested to obtain these materials, hinting at the importance of ochre in the human activities at the site.

Faunal remains

The studied faunal sample ($n = 191$) is dominated by ungulate remains (88%; Extended Data Table 5 and Supplementary Section 13). Among the ungulates, four taxa are almost evenly represented: aurochs (*Bos primigenius*), equids (*Equus* spp.), Mesopotamian fallow deer (*Dama mesopotamica*) and mountain gazelle (*Gazella gazella*). The equid remains are variable in size and probably represent two coexisting forms. Wild boar (*Sus scrofa*), red deer (*Cervus elaphus*) and caprine remains were also found, the latter most likely belonging to the bezoar goat, *Capra aegagrus*. A rhinoceros phalanx completes the ungulate

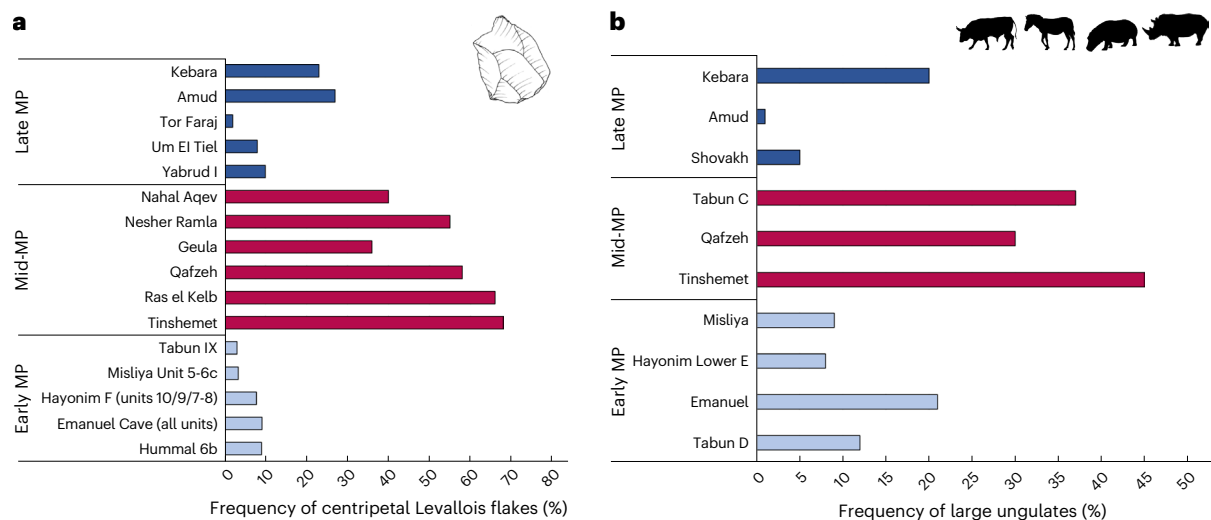


Fig. 6 | Centripetal Levallois method and large-game hunting in the Levantine MP. a, Frequencies of Levallois flakes with centripetal scar patterns on the dorsal faces in various Levantine MP assemblages. The data and references are provided in Supplementary Table 7. **b**, The relative abundance of the largest ungulates (aurochs, equids, rhino and hippo) among the MP cave sites. The data

and references are provided in Supplementary Table 9. Credit: Silhouettes from PhyloPic under a Creative Commons license [CC0 1.0](https://creativecommons.org/licenses/by/4.0/): horse, Lisa Nicvert; deer, Feeran Sayol; aurochs, Mariana Ruiz Vilarreal; hippo, Steven Traver; rhino, Jody Taylor.

repertoire. Two large carnivore remains were found; one was identified as a calcaneus of a hyeanid. Isolated remains of porcupine (*Hystrix* sp.), small to medium-sized birds (yet unidentified), spur-thighed tortoise (*Testudo graeca*), and lizard and snake vertebrae complete the taxonomic spectrum. Taphonomic analysis has yet to be performed, but humans may be considered the primary (but probably not exclusive) accumulation agent; some hammerstone percussion notches were observed on limb bones, as well as a few cases of carnivore damage.

Differences were observed between faunal samples from three depositional contexts: the Terrace (Units A–B), the outer part of the First Chamber (Layers II–III) and the DB Layer. While our sample remains small, these contexts significantly differ in the relative abundance of the four most common taxa ($\chi^2 = 13.17$, d.f. = 6, $P = 0.04$; weak to moderate effect size, Cramer's $V = 0.24$). The variability is driven by the absence of equids in the DB Layer and the relatively low *Dama* proportions in the Terrace. Overall, the Terrace (all units combined) is dominated by gazelle, aurochs and equids, while Layer III of the First Chamber also includes *Dama* in a significant proportion (Extended Data Table 5 and Supplementary Section 13).

Human remains

Human remains, totalling five individuals, were discovered in different layers of Tinshemet Cave. Notable findings include two fully articulated skeletons, three isolated skulls in varying states of preservation, assorted appendicular bones and isolated teeth. Ongoing investigations focus on the remains recovered from Units A and B1a on the Terrace and in Layer III of the First Chamber. Tinshemet Cave fossils are still under study and are preliminarily characterized as *Homo* spp.

The comprehensive analysis of several of the burials at Tinshemet Cave, including a burial of a nearly complete adult skeleton (Tinshemet 2; Fig. 5) from Unit B1a, a burial of a nearly intact child skeleton (Tinshemet 1) from Layer III of the First Chamber and a partially exposed burial (Tinshemet 8) from Unit A2, has unravelled important findings about funerary practices and interment processes at Tinshemet Cave. These include formal inhumation of both adults and children, and the fetal or sleeping position of the dead (bodies lying on their sides with highly flexed legs, arms bent towards the chest and face, and the head facing down; Fig. 5). The dominance of primary burials (on the basis of the fully or partial articulated skeletons) suggests immediate burial

after death. Additional insights into the burial practices at Tinshemet Cave suggest grave inclusions—that is, large pieces of ochre (Fig. 4b).

Discussion

Lithic technologies as a measure of inter-population connectivity

The centripetal Levallois technology is the dominant lithic reduction method used at Tinshemet Cave, as at all other mid-MP sites (Fig. 6a), with unidirectional convergent Levallois point production representing an auxiliary knapping method (Supplementary Section 14)^{28,29,34,52–54}. The neighbouring northern part of the Arabian Peninsula shows similar technological features^{27,55} and is probably part of the same techno-complex²⁹. Precursor early MP (~250–140 ka) lithic industries of the Levant exhibit an entirely different technological set than that of the Levantine mid-MP, with the dominance of blades produced by non-Levallois laminar methods and the production of Levallois blanks employing convergent unidirectional and bidirectional methods^{56–58}. The Levantine early MP industries display no evidence of the systematic use of the centripetal Levallois method, which became dominant in the Levant in the mid-MP (Fig. 6a and Supplementary Section 14). The centripetal Levallois method persisted into the late MP (80–45 ka), where it occurs alongside other Levallois as well as non-Levallois and laminar methods, but rarely dominates the lithic assemblages (but see refs. 59–62). The Levantine mid-MP lithic technological homogeneity differs from the neighbouring regions, such as the technologically heterogeneous East Africa during the Middle Stone Age^{28,29,63–65}. The technological homogeneity that occurs across *Homo* groups in south-west Asia suggests high inter-population connectivity within this region during the mid-MP²⁹.

Ochre—a marker of socially mediated activities

During the mid-MP, ochre emerged as an important cultural substance whose exploitation is likely to have involved trips to distant sources and heat treatment (Supplementary Sections 12 and 15). The use of ochre in the Levantine MP was reported only in mid-MP sites roughly contemporaneous with Tinshemet Cave. Its use has been linked to funerary practices²² and has been taken as evidence of a human behavioural mode probably undergirded by the emergence of symbolic thought. For instance, at Qafzeh Cave, the quantity of ochre increases in Layer

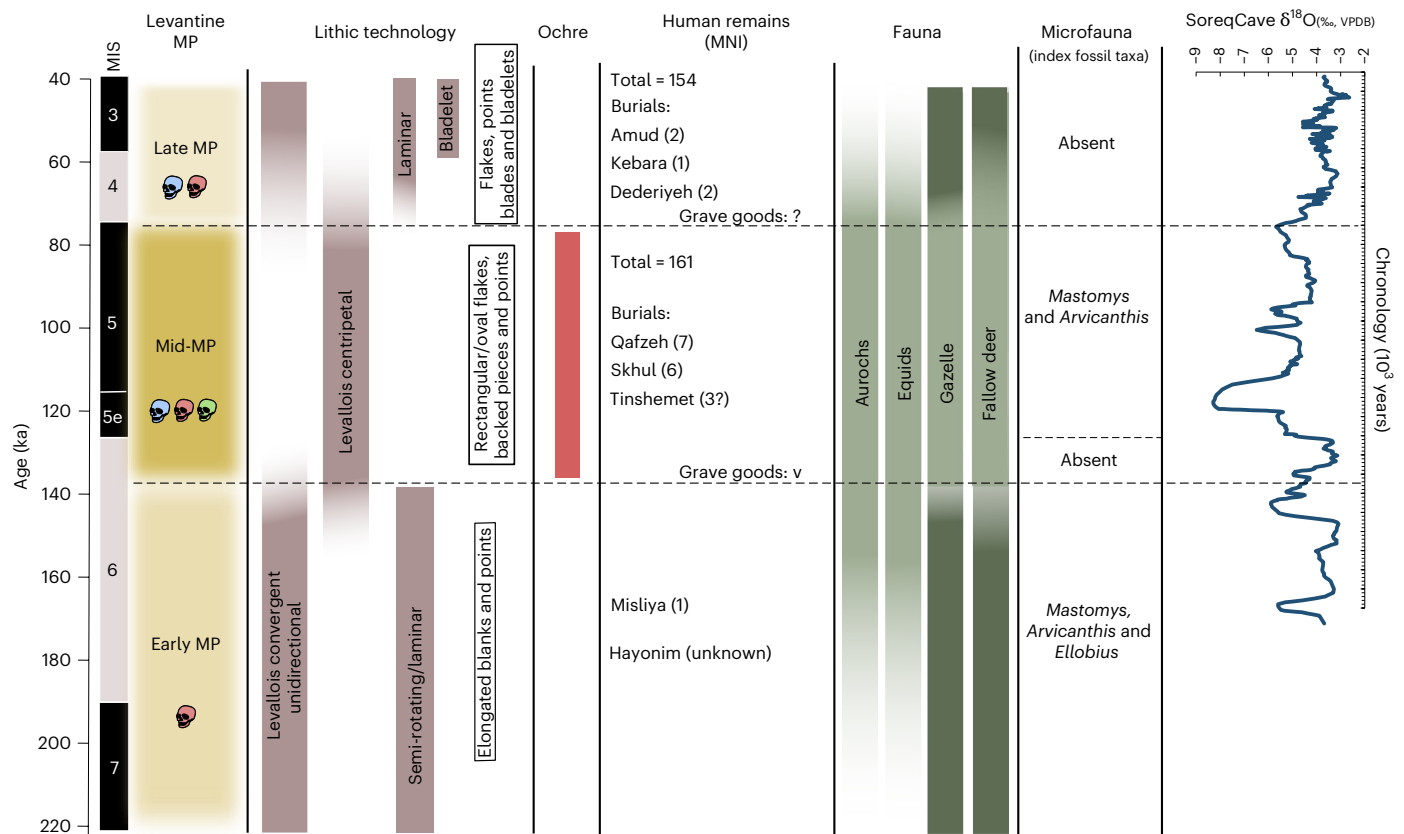


Fig. 7 | Cultural and environmental characteristics of the Levantine MP. The different proxies that characterized the Levantine MP. The mid-MP differs from the early and late MP in lithic production methods, symbolic behaviour (the

use of ochre and burial practices) and hunting strategies. VPDB, Vienna Pee Dee belemnite; v, present. Credit: Skull icon adapted from OpenClipArt under a Creative Commons license [CC0 1.0](https://creativecommons.org/licenses/by/4.0/).

XVII, where most burials are located. Some particular associations between ochre and burials were also reported (that is, burial 8), whereas the concurrent disappearance of both burials and ochre above Layer XVII at Qafzeh Cave is striking²². The ochre chunks at Skhul Cave were retrieved from Layer B2, where human burials were found. Ochre also occurs in mid-MP sites that lack burials, including Nesher Ramla, Israel, where it is found throughout the stratigraphic sequence, and at Nahr Ibrahim, Lebanon⁶⁶.

Heating of the ochre to obtain red colour, reported at Skhul, Qafzeh and Tinsihmet, is likely to be related to the importance of red in symbolic communication^{22,24,67–71}. Ochre stain was also found on perforated marine shells from Qafzeh, which are likely to have been used as personal ornaments²³. An additional aspect of ochre use is the long-distance trips involved in its acquisition²⁴.

Exploitation of large ungulates

From the perspective of game exploitation, the mid-MP displays a consistent pattern that differs from those of the early and late MP in the region (Supplementary Section 16). The data show a more even representation of species and increased reliance on large-bodied ungulates in the mid-MP compared with the early and late stages of the Levantine MP. The proportion of the largest ungulate prey taxa, aurochs and equids, at Qafzeh, Skhul, Tabun C, Tinsihmet Cave and the open-air site of Nesher Ramla^{72–74} is consistently greater than during the earlier and later stages of the MP, especially in respect to cave sites^{75–79} (Fig. 6b). A game exploitation system focused on the largest prey species in the landscape may reflect a shift in human prey choice or may be linked to a major behavioural change in carcass transport patterns associated with different settlement and site-use strategies. It is also possible that the specialized funerary activity that occurred in

some of these sites impacted the archaeofaunal pattern—for example, by focusing on consuming the largest animals in the landscape (an issue discussed in a much later context⁸⁰).

Funerary practices

The Tinsihmet burials present an exceptional opportunity for comparative analysis of burial customs across prominent mid-MP Levantine sites. All three major Levantine mid-MP sites with skeletal remains, Tinsihmet Cave (MNI = 5), Skhul Cave (MNI = 10) and Qafzeh Cave (MNI = 25), fall within the multiple-burials site category^{4,81}, signifying that a major activity at these sites involved the deliberate treatment and deposition of the deceased. The cultural responses to death were similar in all three sites. All three sites show remarkable similarities in how people disposed of their dead. These characteristics include the highly flexed position of the deceased (Fig. 5) and the placement of various objects inside the grave, including animal remains and chunks of ochre^{4,7,20,21,52,82,83}, which demonstrate similarities in symbolically mediated behaviour across these sites and suggest that the intricacy of funerary rites in the mid-MP surpasses that of late MP burials of Levantine Neanderthals exposed at Amud and Kebara Caves, dating to 70–50 ka^{84,85}. The mid-MP burials at Tinsihmet, Qafzeh and Skhul caves represent the earliest instances of intentional *Homo* burials, predating the formalized burial practices in Europe and Africa by tens of thousands of years^{86,87}.

Behavioural uniformity across *Homo* groups

The consolidation of a unified behavioural package during the ~50,000-year-long Levantine mid-MP deserves particular attention as it stands in stark contrast to the heterogenous morphology of the local hominin population. The MP Levant was inhabited by three

hominin groups: archaic Neanderthal-like *Homo*, Neanderthals and *H. sapiens*^{3,5,6,88–94}. The evidence suggests that some of these hominins coexisted. The site of Nesher Ramla yielded *Homo* remains that bear a combination of Neanderthal and archaic *Homo* features, which chronologically overlap with the Qafzeh and Skhul fossils^{5,29,38,95,96}. The stratigraphic position and chronometric age of the Tabun C1 pre-Neanderthal/Neanderthal skeleton are controversial, although some authors suggest a mid-MP age for the fossil^{39,97–100} (but see ref. 101). The identification of the Skhul/Qafzeh group as a single population of archaic *H. sapiens* is also debated. The identification of the Skhul specimens as modern humans was supported by some scholars^{15,17,102}, while others identified them as a separate morphological group or as hybrids^{3,18,19,103–105}, emphasizing their peculiar characteristics in the morphology of the chin and the brow ridges^{3,8–10,106,107}, and the morphological differences between the Skhul and Qafzeh fossils^{8–10}. The morphological variability of the Qafzeh hominins is also notable^{6,12}, including fossils that show characteristics that do not align with *H. sapiens*^{8,10,13,14}. Noticeably, all Qafzeh fossils occur in the same archaeological context, close to each other within the site's stratigraphy.

The morphological variability of the Levantine MP hominins has become a source of heated debate on their taxonomic identity and on the question of *H. sapiens* and Neanderthal interactions in the region. The hypotheses raised include coexistence with no interactions¹⁰⁸, alternating occupations^{17,109}, brief episodes of engagement followed by extinction³², and interactions that facilitated cultural transmission and assimilation across species^{29,106,110}. The final scenario is supported by recent studies of the facial and dental morphology of the Qafzeh and Skhul fossils that show that the Qafzeh and Skhul hominins fall well within the expected morphology of hybrid populations^{11,18,111,112}, supporting previous similar views^{3,13,19,104,106,107}. A recent study based on the lithic technological behaviour of the Nesher Ramla hominins demonstrated that Nesher Ramla, Skhul and Qafzeh shared core reduction technologies, suggesting that cultural diffusion and interaction across *Homo* populations is the most likely reason for the close cultural similarity between these sites²⁹. The behavioural evidence from Tinsmet Cave further supports a high level of inter-population connectivity in the Levantine mid-MP. The summary of the MP human behavioural features in the Levant presented in Fig. 7 reveals a well-defined mid-MP entity with a widely shared behavioural repertoire found across the four major Levantine sites (Qafzeh, Skhul, Nesher Ramla and Tinsmet) with chronological overlaps (Supplementary Sections 14–16). These strata broadly share a uniform lithic technology, the use of ochre, a large-ungulate hunting pattern, the presence of articulated human remains and the presence of grave goods or non-utilitarian artefacts^{113,114}. We suggest that the association between behavioural uniformity and high human biological variability could be a result of intensifying social interactions and admixture among African *H. sapiens* and Eurasian Neanderthal-like hominins in the mid-MP Levant. It is now increasingly understood that several taxa provided population sources for the Levantine MP and that population influxes from different sources chronologically overlapped in a way that created opportunities for genetic and social admixtures^{5,11,18,29,115}.

Methods

Excavation

The fieldwork consisted of the excavation of 5-cm-thick spits in 0.5 m × 0.5 m squares. Each flint artefact longer than 2 cm, bones longer than 3 cm, ochre larger than 0.5 cm, ground stone tools, charcoals, shells and all human remains were recorded with a total station. The excavation of the cemented deposits was conducted using pneumatic tools (PaleoTool), die grinders, electric hammers and hand chisels. The deposits were softened with water. This combination of techniques allowed us to extract complete artefacts and bones and perform 3D measurements.

Geoarchaeology

Mineralogical identification was conducted on 307 sediment samples using Fourier transform infrared spectroscopy with the well-established KBr method (ref. 116, Ch. 12). Phytoliths and wood ash pseudomorphs were extracted and quantified from 68 sediment samples (~22% of the total samples) following the procedures of Katz et al.¹¹⁷ and Gur-Arie et al.¹¹⁸. Phytoliths and wood ash pseudomorphs were sought to obtain information on plant use and combustion activities by hominins. Small (<5 mm) fragments of bones ($n = 141$) found in sediment samples were assigned to burn colour codes, which were verified using Fourier transform infrared spectroscopy following the guidelines outlined in Stiner et al.¹¹⁹.

Monolithic blocks for micromorphological examination were sampled along the sedimentary sequence, impregnated by polyester resin, cut and ground to 30 µm thickness according to established procedures. A total of 43 thin sections were produced and studied using a Nikon petrographic microscope.

The particle size distribution of the detrital grains (nine carbonate-free samples) was analysed using a Malvern 3000 laser diffraction analyser following Crouvi et al.¹²⁰. The samples were then examined using a binocular, scanning electron microscopy, and energy dispersive spectroscopy.

TL dating

Among the flint samples showing evidence of past heating and therefore selected for TL dating¹²¹, 20 have signals that had been reset in the past according to preliminary TL tests. Ten samples come from the Terrace, from squares AD23, AE23, AF23, AF24 and AE25; they are associated with Units B1a, B1b and C. The other ten samples were unearthed from Layer III in the First Chamber, at the entrance of the cavity, in squares AO19, AO20, AM20, AM21 and AN21, and from the DB Layer (squares AO18 and AN18).

Current gamma and cosmic dose rates have been measured with dosimeters¹²² buried for months at different locations and at different depths in the Terrace and the First Chamber. Their analysis following Kreutzer et al.¹²³ lead to gamma dose rates ranging from 357 to 454 µGy/a for the Terrace, and from 361 µGy/a at the entrance of the First Chamber to 551 µGy/a deeper in the cavity (Supplementary Table 2). For each flint, the gamma dose rate used for the TL age calculation was then obtained by averaging the values recorded by the nearest dosimeters, and considering a past moisture content of $10 \pm 3\%$ on average for the Terrace sediments and of $15 \pm 4\%$ for the sediments of the First Chamber. Cosmic dose rates were computed following Prescott and Hutton¹²⁴ considering, for the Terrace, the thickness of sediments at the time of the first excavation, and the protection induced by the shelter for samples coming from the First Chamber.

For each flint, the alpha and beta dose rates were deduced from its radioactive content in U, Th and K, which was determined via ICP-MS on a fraction (100 mg) of the powder prepared for the TL measurements.

Overall, the total dose rate ranges from about 700 to 3,800 µGy/a, including an external fraction that varies greatly from sample to sample and represents 22–81% of the total (Extended Data Table 1).

After extraction by sawing with a diamond saw, the core of each flint, which was thus externally irradiated only by gamma and cosmic rays, was prepared following the recommendations of Valladas¹²⁵. TL measurements were done using coarse (100–160 µm) grains dispersed on stainless-steel cups and performed with a TL reader to which a calibrated ⁹⁰Sr beta source was fitted and used for delivering artificial doses¹²⁶. The additive dose technique was applied to describe the growth of the TL signal, integrated between 330 and 430 °C, as a function of the total dose received (natural + artificial). The same technique was also applied to a fraction of the natural powder reset by heating at 350 °C for 90 min: the measurement of regenerated TL signals thus allowed the description of the growth curve in the low dose range. The palaeodose values deduced from the analysis of the individual

growth curves range from 56 to 477 Gy (Extended Data Table 1) and increase as a function of the internal (alpha and beta) dose rate (Supplementary Fig. 1).

OSL

OSL uses the dosimetric properties of quartz to date the most recent exposure of the grains to sunlight. When buried, quartz accumulates a signal due to the natural radiation emitted from radioactive elements in the sediment. When exposed to sunlight, this signal is reset ('zeroed'), and it accumulates once more after burial. This signal is measured in the lab, and the OSL intensity is compared to laboratory-induced OSL created by artificial beta doses (the equivalent dose, or D_e). The burial age is determined by the ratio between the D_e and the environmental dose rate measured in the surrounding rocks.

The limestone bedrock at Tinsmet Cave does not contain any quartz. The source of all the quartz found in the deposits in the cave and on the Terrace (which had also been part of the cave) is aeolian, blown in from the coast or the southern desert by strong winds. The grain size of this quartz is silt to very fine sand, and the latter is sufficiently coarse to be used for OSL coarse-grain dating¹²⁷.

Twenty-four samples for OSL dating were collected at the site during three excavation seasons from all areas and layers (Extended Data Table 2). Due to the indurated character of the sediments on the Terrace, samples were collected as blocks cut from the breccia using a diamond saw. The blocks were further cleaned in the laboratory under safe amber light. In the inner chamber, the softer sediments were sampled either by drilling with a hand-held auger or, when rocks interfered, with a gardening trowel. All samples were placed immediately in light-tight black bags to avoid any exposure to sunlight. One or two additional samples were collected from each location for dose-rate evaluations.

The surfaces of the breccia blocks were first cleaned of grains that might have been exposed to the sun by soaking them in diluted hydrochloric acid (8% HCl), which dissolved the cementing calcite, followed by scrubbing with a metal brush. The cleaned blocks were then placed in light-tight bags and crushed using a pneumatic press. The diminished material was then placed in diluted HCl for several days until a sufficient amount was dissolved and enough quartz was released from the breccia. The samples were washed and sieved to 75–125 μm , the most common sand-size fraction in the sample.

The sediment samples from the chamber were processed using routine laboratory procedures. Wet sieving was used to isolate the 75–125 μm fraction, followed by soaking in HCl to remove carbonates, followed by rinsing and drying. This fraction from all the samples was passed through a Frantz magnetic separator to remove heavy minerals and some feldspars. The grains were etched in 40% HF for 40 min to dissolve the remaining feldspars and remove the outer rim of the grains, followed by soaking overnight in 16% HCl to remove any fluorides that may have precipitated. After thorough rinsing and drying, the samples were ready for measurements.

The additional samples for dose-rate evaluations were crushed, homogenized and split, and a representative ~50 g subsample was powdered. The concentrations of uranium (U) and thorium (Th) were measured using ICP-MS, whereas potassium (K) was measured by ICP-optical emission spectrometry. For each sample, two or more analyses were carried out, either from duplicate samples taken at the site or from duplicated measurements of one powdered fraction. Alpha, beta and gamma dose rates were evaluated from the concentrations of the radioactive elements using attenuation factors of Nambi and Aitken¹²⁸. Gamma dose rates were also evaluated from aluminium oxide dosimeters placed in the locations of the flint samples (see 'TL dating') in cases where they were within 30 cm of the OSL sample. The gamma dose rates to samples were weighted from the dosimeters and the values calculated from the chemical analyses, according to the distance between the OSL sample and the dosimeter. Moisture contents

of $10 \pm 3\%$ and $15 \pm 4\%$ were estimated for the Terrace and chamber sediments, respectively. Cosmic dose rates were evaluated following Prescott and Hutton¹²⁴ and considering the additional 0.6 m of topsoil removed during excavations on the Terrace, and the rock overburden for the samples from the chambers.

The quartz D_e values were measured on 17–20 2-mm aliquots for each sample. Five dose points were used to construct the dose response curve, including a zero point and a repeated (recycling) point. The sample average D_e was calculated using the central age model, which assumes that all grains in a sample have the same depositional age and absorbed the same dose¹²⁹.

A dose recovery test over a range of preheat and cutheat temperatures showed that a recovery ratio of 0.99 can be obtained under a preheat of 10 s at 260 °C, a test dose of 8 Gy and a test dose cutheat of 5 s at 220 °C (Supplementary Fig. 1a). These measurement conditions were used for all samples.

The OSL signal of all the samples is bright and decays to background level within 2–3 s; the dose response curves can be well fitted with an exponential + linear fit, and recycling ratios are mostly within 5% of unity. The distribution of the measured aliquots is usually normal with low overdispersion values, justifying the use of the central age model (Extended Data Table 2 and Supplementary Fig. 2).

U-series dating on flowstones and snail shells

The U-series dating method was applied to two flowstones from the top of Unit A and to six fragments of snail shells unearthed from the Terrace: two from Unit B1a (Tin19SSh1 and 2) and four from Unit B1b (Tin19SSh6 to 9). The samples were prepared following the protocol described in Martin et al.⁴⁸. All the samples were first embedded in resin (Araldite 2020), cut into slices in a horizontal plane and dry polished to obtain a flat surface suitable for LA sampling.

The measurement of isotopes relevant for U-series dating (²³⁸U, ²³⁵U, ²³⁴U, ²³⁰Th and ²³²Th) was made by coupling a femtosecond LA system (Lambda 3, Nexeya SA/Amplitude System) with a sector field (SF) ICP mass spectrometer (SF-ICPMS Element XR, Thermo Scientific). LA sampling was carried out using adjacent sub-parallel transects of 30 μm height, with a horizontal displacement speed of 30 $\mu\text{m s}^{-1}$, resulting in 2D imaging of the isotopes' distribution within each analysed section with a resolution of 30 \times 30 μm^2 per pixel (one measure of each isotope per second). Two to five replicas were made for each sample, for a total ablated mass ranging from 2.6 to 4.9 mg for speleothems and 0.5 to 3.2 mg for snail shells. The FsLA SF-ICP-MS coupling sensitivity was optimized daily by measuring a certified glass (NIST612) while maintaining a U/Th ratio of 1.00 ± 0.05 to ensure efficient particle atomization into the SF-ICP-MS plasma. Oxide corrections (<0.23% for both ThO/Th and UO/O), mass bias correction and background correction were considered. The images were processed with ImageJ (v. 1.53)¹³⁰. Their analysis aimed to identify areas affected by recrystallization or polluted by exogenous materials (then defined as the region of exclusion) and to calculate isotope ratios and ages only in the preserved areas (regions of interest). For more details about the protocol used, equipment optimization and data processing, refer to A. Galy et al. (manuscript in preparation).

Cryptotephra

Samples for cryptotephra analyses were collected at 5 cm intervals from existing and freshly cleaned profiles under active excavation at the site. A total of 43 bulk sediment samples were taken from 5 sampling columns (Supplementary Section 8 and Supplementary Figs. 3 and 4). On the Terrace, within the cemented sediments (Supplementary Fig. 3), samples from Columns 1–4 were collected using a rotary power saw with a 5-cm-diameter blade. Columns 1 and 2 were located in Square AI24 (east profile), with Column 1 extending from the site surface to a depth of 40 cm (88.04–87.64 m datum) and Column 2 stepped immediately below, extending a further 40 cm (87.61–87.21 m datum)

and reaching the contact between the very hard breccia and Unit B1. Column 3 was located in Square AD24 (west profile) in a transitional position between Column 2 and Column 4, spanning a 25 cm sequence of sub-units B1a and B1b (86.92–86.67 m datum). Column 4 included two overlapping sections, designated as Columns 4A and 4B, within Square AG25 (east profile). Column 4A extended 30 cm (86.78–86.48 m datum) from Unit B1a to the B1b/C contact. The adjacent Column 4B measured 20 cm (86.44–86.24 m datum), extending from the Unit B1/C contact a further 15 cm into Unit C. Within the cave's First Chamber, Column 5 also comprised two overlapping sections, including Columns 5A and 5B (Square AM21, south profile), each spanning 30 cm (87.11–86.81 m and 87.26–86.96 m datums, respectively) of the unconsolidated sediment sequence designated as the 'light brown' Layer III (Supplementary Fig. 4).

In the laboratory, the samples were immersed in 10% HCL to dissolve the carbonate fraction. Residual material was passed through disposable nylon sieve meshes, retaining the intermediary fraction between 125 and 15 µm. This material was subjected to a standard density separation procedure based on Blockley et al.¹³¹, which preferentially removes organic detritus and concentrates volcanic glass shards of a more felsic chemical composition. The remaining material following the density separation phase was mounted onto glass slides using Canada balsam and examined under a polarizing light microscope. Glass shard identification was undertaken manually at ×100 and ×400 magnification. Glass shards for major and minor elemental analysis were extracted from a water mount using a mechanical 'picking' device and embedded in an epoxy resin. Major and minor elemental analyses were conducted using a Cameca Electron Probe Microanalyser housed at the Tephra Analysis Unit, University of Edinburgh. Probe conditions and procedures followed the guidelines of Hayward¹³².

Lithic technology and use-wear studies

The number of lithic artefacts retrieved so far at Tinsmet Cave is approximately 10,000 (>2 cm). The sample of lithic material studied here is about 30% of the total assemblage. The sample comprises ~800 artefacts from the squares most dense in lithic artefacts in the First Chamber (AM 21-22 and AN 21) and almost 2,000 artefacts from the densest squares on the Terrace (AF 23-24-25 and AE 23-24-25). Both samples represent complete assemblages excavated from about 1-m-thick archaeological deposits. For both assemblages, flint artefacts found within the topsoil layer were excluded from the analyses. The lithic study encompassed attribute analyses and general observations related to the *chaîne opératoire* concept, such as raw material identification, state of preservation, blank types and scar patterns. The typology follows the traditional Bordes list¹³³.

Forty-four flint artefacts were inspected to check the preservation of use-wear. Sample selection was done including bone retouched and unretouched items. All artefacts were analysed at the TraCER laboratory (Neuwied, Germany) using a stereo-microscope (ZEISS SterEO Discovery V8), a digital microscope (Zeiss Smartzoom 5) and a metallographic microscope (Zeiss-Axio ScopeA1). The magnification ranged from ×10 to ×50 with the stereomicroscope and digital microscope and from ×50 to ×500 with the metallographic microscope. Extended depth-of-focus images were created using the post-processing software Helicon Focus (v. 8.0.2).

The analysis under low magnification focused mainly on the observation of macro-wear (scars and edge rounding) and on the possible identification of ancient residues. The analysis with a metallurgical microscope allowed a more detailed analysis of wear patterns, such as polish and striations¹³⁴. Interpretations relied on comparisons with published images found in the literature^{134–136}.

Micromammal remains

Remains of micromammals were retrieved for analysis from soft-sediment deposits; further analysis of material extracted from

well-brecciated contexts will require considerably more time and effort. A fair sample size of 229 molar teeth of micromammals (rodents and insectivores) was obtained for a preliminary taxonomic description of the assemblage in the present study. This sample represents a relatively limited spatial coverage compared with the entire area of exposed archaeological deposits (retrieved from 9 out of the 150 m²). It is, however, representative of the different excavation contexts, including material from within and outside the present extent of the cave and from some of the excavation squares in which human remains were uncovered.

Palynology study

Eleven samples were taken during seasons 2021 and 2022 using sterile equipment to prevent outside contamination (Supplementary Table 4). Eight samples were recovered from archaeological layers (sample nos. 1–8), and one sample was collected from a compact layer located at the lowest archaeological stratum (sample no. 9). This sample was characterized by a yellowish-greyish colour. Two additional samples were collected to serve as controls (sample nos. 10 and 11): one sample from the surface sediment, 20 m northeast of the cave, and one sample of recent guano collected from the inner part of the cave.

Laboratory procedure. The pollen extraction process began with soaking the samples in 32% HCL for ten days, combined with 1 min of sonication per day. This physical–chemical treatment removes the calcium carbonates within the samples, loosens the different compact debris and dissolves the *Lycopodium* spores (a tracer added at the beginning of the process that enables us to calculate pollen concentrations¹³⁷). The samples were then rinsed with distilled water several times until pH 7 was achieved. Next, a density separation was performed using ZnBr₂ solution with a specific gravity of 1.95. After mixing and vortex, the samples were placed in an ultrasonic water bath for 2 min. After sonication, the samples were centrifuged for 20 min at 3,500 rpm (all other steps were followed by only 5 min of centrifuging at the same rpm). The floated suspension was sieved through a 150 µm mesh screen and rinsed with distilled water. After sieving (150 µm mesh screen), the unstained residues were homogenized and mounted onto microscope slides using glycerin. The control sample of the recent fruit bat guano (sample no. 11) passed through a short acetolysis process after sieving due to its high organic content.

Pollen identification. Pollen grains were identified under a light microscope at magnifications of ×200, ×400 and ×1,000 (oil immersion) to the most detailed possible systematic level. For pollen identification, a comparative reference collection at Tel Aviv University (Steinhardt Museum of Natural History) was used, in addition to pollen atlases^{138–141}. When possible, all the extracted pollen grains were counted and identified.

Reporting summary

Further information on research design is available in the Nature Portfolio Reporting Summary linked to this article.

Data availability

The data are provided in the main text, Extended Data Figures and Tables, and Supplementary Information. The lithic, ochre and micromammal assemblages of Tinsmet Cave are housed in the Institute of Archaeology at the Hebrew University of Jerusalem. The faunal remains are stored at the Zinman Institute of Archaeology and the School of Archaeology and Maritime Cultures, University of Haifa. The human remains are stored at the Dan David Center for Human Evolution and Biohistory Research, Faculty of Medicine, Tel Aviv University. Archaeological materials are accessible for all researchers upon request.

References

- Bae, C. J., Douka, K. & Petraglia, M. D. On the origin of modern humans: Asian perspectives. *Science* **358**, eaai9067 (2017).
- Freidline, S. E. et al. Early presence of *Homo sapiens* in Southeast Asia by 86–68 kyr at Tam Pà Ling, Northern Laos. *Nat. Commun.* **14**, 3193 (2023).
- McCown, T. D. & Keith, A. *The Stone Age of Mt. Carmel II: The Fossil Human Remains from the Levallois-Mousterian* (Oxford, 1939).
- Vandermeersch, B. & Bar-Yosef, O. The Paleolithic burials at Qafzeh Cave, Israel. *PALEO* <https://doi.org/10.4000/paleo.4848> (2019).
- Hershkovitz, I. et al. A new Middle Pleistocene *Homo* from Nesher Ramla, Israel. *Science* **372**, 1424–1428 (2021).
- Vandermeersch, B. *Les Hommes Fossiles de Qafzeh (Israël)* (CNRS, 1981).
- Vandermeersch, B. in *The Transition from the Lower to the Middle Palaeolithic and the Origin of Modern Man* Vol. 151 (ed. Ronen, A.) 297–300 (BAR International Series, 1982).
- Schwartz, J. H. & Tattersall, I. *The Human Fossil Record, Craniodental Morphology of Genus Homo (Africa and Asia)* Vol. 2 (Wiley, 2003).
- Klein, R. G. Archeology and the evolution of human behavior. *Evol. Anthropol.* **9**, 17–36 (2000).
- Corruccini, R. S. Metrical reconsideration of the Skhul IV and IX and Border Cave 1 crania in the context of modern human origins. *Am. J. Phys. Anthropol.* **87**, 433–445 (1992).
- Harvati, K. & Ackermann, R. R. Merging morphological and genetic evidence to assess hybridization in Western Eurasian late Pleistocene hominins. *Nat. Ecol. Evol.* **6**, 1573–1585 (2022).
- Tillier, A.-M. *Les Enfants Moustériens de Qafzeh: Interprétation Phylogénétique et Paléoauxologique* (Cahier de Paleoanthropologie, 1999).
- Vallois, H. V. & Vandermeersch, B. The Mousterian skull of Qafzeh (*Homo VI*): an anthropological study. *J. Hum. Evol.* **4**, 445–455 (1975).
- Simmons, T., Falsetti, A. B. & Smith, F. H. Frontal bone morphometrics of southwest Asian Pleistocene hominids. *J. Hum. Evol.* **20**, 249–269 (1991).
- Stringer, C. B. in *Origins of Anatomically Modern Humans* (eds Nitecki, M. H. & Nitecki, D. V.) 149–172 (Springer US, 1994); https://doi.org/10.1007/978-1-4899-1507-8_8
- Trinkaus, E. The Neandertals and modern human origins. *Annu. Rev. Anthropol.* **15**, 193–218 (1986).
- Rak, Y. in *Species, Species Concepts and Primate Evolution* (eds Kimbel, W. H. & Martin, L. B.) 523–536 (Springer US, 1993); https://doi.org/10.1007/978-1-4899-3745-2_20
- Churchill, S. E., Keys, K. & Ross, A. H. Midfacial morphology and Neandertal–modern human interbreeding. *Biology* **11**, 1163 (2022).
- Eiseley, L. C. Missing link or hybrid—which? *Prairie Schooner* **20**, 250–256 (1946).
- Vandermeersch, B. Une sépulture moustérienne avec offrandes découverte dans la grotte de Qafzeh. *C. R. Acad. Sci.* **268**, 298–301 (1970).
- Belfer-Cohen, A. & Hovers, E. In the eye of the beholder: Mousterian and Natufian burials in the Levant. *Curr. Anthropol.* **33**, 463–471 (1992).
- Hovers, E., Ilani, S., Bar-Yosef, O. & Vandermeersch, B. An early case of color symbolism: ochre use by modern humans in Qafzeh Cave. *Curr. Anthropol.* **44**, 491–522 (2003).
- Bar-Yosef Mayer, D. E., Vandermeersch, B. & Bar-Yosef, O. Shells and ochre in Middle Paleolithic Qafzeh Cave, Israel: indications for modern behavior. *J. Hum. Evol.* **56**, 307–314 (2009).
- d’Errico, F., Salomon, H., Vignaud, C. & Stringer, C. Pigments from the Middle Palaeolithic levels of Es-Skhul (Mount Carmel, Israel). *J. Archaeol. Sci.* **37**, 3099–3110 (2010).
- Hovers, E. *The Lithic Assemblages of Qafzeh Cave* (Oxford Univ. Press, 2009).
- Bar-Yosef, O. in *Neandertals and Modern Humans in Western Asia* (eds Akazawa, T. et al.) 39–56 (Plenum, 1998); https://doi.org/10.1007/0-306-47153-1_3
- Groucutt, H. S. et al. Stone tool assemblages and models for the dispersal of *Homo sapiens* out of Africa. *Quat. Int.* **382**, 8–30 (2015).
- Prévost, M. & Zaidner, Y. New insights into early MIS 5 lithic technological behavior in the Levant: Nesher Ramla, Israel as a case study. *PLoS ONE* **15**, e0231109 (2020).
- Zaidner, Y. et al. Middle Pleistocene *Homo* behavior and culture at 140,000 to 120,000 years ago and interactions with *Homo sapiens*. *Science* **372**, 1429–1433 (2021).
- Petraglia, M. D. et al. Hominin dispersal into the Nefud Desert and Middle Palaeolithic settlement along the Jubbah Palaeolake, northern Arabia. *PLoS ONE* **7**, e49840 (2012).
- Shea, J. J. Neandertals, competition, and the origin of modern human behavior in the Levant. *Evol. Anthropol.* **12**, 173–187 (2003).
- Shea, J. J. Transitions or turnovers? Climatically-forced extinctions of *Homo sapiens* and Neanderthals in the east Mediterranean Levant. *Quat. Sci. Rev.* **27**, 2253–2270 (2008).
- Weissbrod, L. & Weinstein-Evron, M. Climate variability in early expansions of *Homo sapiens* in light of the new record of micro-mammals in Misliya Cave, Israel. *J. Hum. Evol.* **139**, 102741 (2020).
- Barzilai, O. et al. Expansion of Eastern Mediterranean Middle Paleolithic into the Desert Region in early Marine Isotopic Stage 5. *Nat. Sci. Rep.* **12**, 4466 (2022).
- Jelinek, A. J. in *The Transition from Lower to Middle Palaeolithic and the Origin of Modern Man* Vol. 151 (ed. Ronen, A.) 57–104 (BAR International Series, 1982).
- Jelinek, A. J. in *Préhistoire du Levant* (eds Cauvin, J. & Sanlaville, P.) 265–280 (CNRS, 1981).
- Schwarcz, H. P. et al. ESR dates for the hominid burial site of Qafzeh in Israel. *J. Hum. Evol.* **17**, 733–737 (1988).
- Mercier, N. et al. Thermoluminescence date for the Mousterian burial site of Es-Skhul, Mt. Carmel. *J. Archaeol. Sci.* **20**, 169–174 (1993).
- Grün, R. & Stringer, C. Tabun revisited: revised ESR chronology and new ESR and U-series analyses of dental material from Tabun C1. *J. Hum. Evol.* **39**, 601–612 (2000).
- Grün, R. et al. U-series and ESR analyses of bones and teeth relating to the human burials from Skhul. *J. Hum. Evol.* **49**, 316–334 (2005).
- Ambrose, S. H. in *Modern Human Origins and Dispersal* (eds Sahle, Y. et al.) 171–214 (Kerns, 2017).
- Frumkin, A. & Comay, O. The last glacial cycle of the southern Levant: paleoenvironment and chronology of modern humans. *J. Hum. Evol.* **160**, 102609 (2019).
- Centi, L. & Zaidner, Y. The Levallois flaking system in Nesher Ramla Upper Sequence. *J. Paleolit. Archaeol.* **4**, 9 (2021).
- Stekelis, M. Preliminary report on soundings in prehistoric caves in Palestine. *Am. Schools Orient. Res.* **86**, 2–10 (1942).
- Frumkin, A., Langford, B., Marder, O. & Ullman, M. Paleolithic caves and hillslope processes in south-western Samaria, Israel: environmental and archaeological implications. *Quat. Int.* **398**, 246–258 (2015).
- García, P., Zaidner, Y., Nicosia, C. & Shahack-Gross, R. Site formation processes at Tinsmet Cave, Israel: micro-stratigraphy, fire use, and cementation. *Geoarchaeology* **40**, e22023 (2025).
- Harel, M., Amit, R., Porat, N. & Enzel, Y. in *Quaternary of the Levant: Environments, Climate Change, and Humans* (eds Bar-Yosef, O. & Enzel, Y.) 433–446 (Cambridge Univ. Press, 2017); <https://doi.org/10.1017/9781316106754.050>

48. Martin, L. et al. Isotopic imaging using fsLA single-collector ICP-SFMS for direct U/Th dating of small archaeological carbonates. *Anal. Chem.* **94**, 3046–3055 (2022).
49. Helama, S., Heikkilä, P., Rinne, K., Nielsen, J. K. & Nielsen, J. K. LA-ICP-MS-derived U-concentrations and microstructural domains within biogenic aragonite of *Arctica islandica* shell. *Environ. Monit. Assess.* **187**, 260 (2015).
50. Zhang, S. et al. Distal tephra reveal new MIS 5e Kos eruptions: implications for the chronology and volcanic evolution histories in the Eastern Mediterranean region. *Quat. Sci. Rev.* **307**, 108054 (2023).
51. Tchernov, E. in *Neandertals and Modern Humans in Western Asia* (eds Akazawa, T. et al.) 77–90 (Plenum, 1998).
52. McCown, T. D. in *The Stone Age of Mount Carmel I* Vol. 1 (eds Garrod, D. A. E. & Bate, D. M. A.) 91–107 (Clarendon Press, 1937).
53. Copeland, L. in *Problems in Prehistory: North Africa and the Levant* (eds Wendorf, F. & Marks, A. E.) 317–350 (Southern Methodist Univ. Press, 1975).
54. Barzilai, O. et al. Rediscovering Geula Cave: a Middle Paleolithic cave site in northern Mt. Carmel, Israel. *Quat. Int.* **624**, 181–197 (2021).
55. Groucutt, H. S. et al. *Homo sapiens* in Arabia by 85,000 years ago. *Nat. Ecol. Evol.* **2**, 800–809 (2018).
56. Meignen, L. & Bar-Yosef, O. Acheulo-Yabrudian and Early Middle Paleolithic at Hayonim Cave (Western Galilee, Israel): continuity or break? *J. Hum. Evol.* **139**, 102733 (2020).
57. Zaidner, Y. & Weinstein-Evron, M. The emergence of the Levallois technology in the Levant: a view from the Early Middle Paleolithic site of Misliya Cave, Israel. *J. Hum. Evol.* **144**, 102785 (2020).
58. Shimelmitz, R. & Kuhn, S. Early Mousterian Levallois technology in Unit IX of Tabun Cave. *PaleoAnthropology* **2013**, 1–27 (2013).
59. Goren-Inbar, N. in *Quneitra: A Mousterian Site on the Golan Heights* Vol. 31, 61–167 (Qedem, Hebrew Univ. Institute of Archaeology, 1990).
60. Oron, M. & Goren-Inbar, N. Mousterian intra-site spatial patterning at Quneitra, Golan Heights. *Quat. Int.* **331**, 186–202 (2014).
61. Abadi, I., Bar-Yosef, O. & Belfer-Cohen, A. Kebara V—a contribution for the study of the Middle–Upper Paleolithic transition in the Levant. *PaleoAnthropology* **2020**, 1–28 (2020).
62. Oron, M., Porat, N. & Hovers, E. Occupation duration and identification of technological traditions: insights from the Late Middle Paleolithic site of Nahal Dimona 24 in the Negev Desert, Israel. *PaleoAnthropology* **2025**, 1–22 (2025).
63. Yellen, J. et al. The archaeology of Aduma Middle Stone Age sites in the Awash Valley, Ethiopia. *PaleoAnthropology* **10**, 25–100 (2005).
64. Douze, K. & Delagnes, A. The pattern of emergence of a Middle Stone Age tradition at Gademotta and Kulkuletti (Ethiopia) through convergent tool and point technologies. *J. Hum. Evol.* **91**, 93–121 (2015).
65. Shea, J. J. The Middle Stone Age archaeology of the Lower Omo Valley Kibish Formation: excavations, lithic assemblages, and inferred patterns of early *Homo sapiens* behavior. *J. Hum. Evol.* **55**, 448–485 (2008).
66. Solecki, R. A ritual Middle Palaeolithic deer burial at Nahr Ibrahim Cave, Lebanon. *MOM Éd.* **12**, 47–56 (1982).
67. Cavallo, G. et al. Heat treatment of mineral pigment during the Upper Palaeolithic in north-east Italy. *Archaeometry* **60**, 1045–1061 (2018).
68. Dapschuska, R., Göden, M. B., Sommer, C. & Kandel, A. W. The emergence of habitual ochre use in Africa and its significance for the development of ritual behavior during the Middle Stone Age. *J. World Prehist.* **35**, 233–319 (2022).
69. Dayet-Bouillot, L., Wurz, S. & Daniel, F. Ochre resources, behavioural complexity and regional patterns in the Howiesons Poort: new insights from Klasies River Main site, South Africa. *J. Afr. Archaeol.* **15**, 20–41 (2017).
70. Pomiés, M.-P., Menu, M. & Vignaud, C. Red Palaeolithic pigments: natural hematite or heated goethite? *Archaeometry* **41**, 275–285 (1999).
71. Salomon, H. et al. Selection and heating of colouring materials in the Mousterian level of Es-Skhu (c. 100 000 years BP, Mount Carmel, Israel). *Archaeometry* **54**, 698–722 (2012).
72. Garrod, D. A. & Bate, D. M. A. *The Stone Age of Mount Carmel* Vol. 1 (Clarendon, 1937).
73. Rabinovich, R., Bar-Yosef, O., Vandermeersch, B. & Horwitz, L. Hominid–carnivore interactions in the Paleolithic site of Qafzeh Cave, Israel. *Rev. Paleobiol.* **23**, 627–637 (2004).
74. Crater Gershtein, K. M., Zaidner, Y. & Yeshurun, R. A campsite on the open plain: zooarchaeology of Unit III at the Middle Paleolithic site of Nesher Ramla, Israel. *Quat. Int.* **624**, 49–66 (2022).
75. Speth, J. D. & Tchernov, E. in *Kebara Cave, Mt. Carmel, Israel: The Middle and Upper Palaeolithic Archaeology, Part I* (eds Meignen, L. & Bar-Yosef, O.) 165–260 (Harvard Univ., Peabody Museum of Archaeology and Ethnology, 2007).
76. Yeshurun, R., Bar-Oz, G. & Weinstein-Evron, M. Modern hunting behavior in the early Middle Paleolithic: faunal remains from Misliya Cave, Mount Carmel, Israel. *J. Hum. Evol.* **53**, 656–677 (2007).
77. Yeshurun, R., Malkinson, D., Crater Gershtein, K. M., Zaidner, Y. & Weinstein-Evron, M. Site occupation dynamics of early modern humans at Misliya Cave (Mount Carmel, Israel): evidence from the spatial taphonomy of faunal remains. *J. Hum. Evol.* **143**, 102797 (2020).
78. Goder-Goldberger, M. et al. Emanuel Cave: the site and its bearing on early Middle Paleolithic technological variability. *Paléorient* **38**, 203–225 (2012).
79. Speth, J. D. in *Kebara Cave, Mt. Carmel, Israel: The Middle and Upper Paleolithic Archaeology, Part II* (eds Meignen, L. & Bar-Yosef, O.) 169–236 (Harvard Univ., Peabody Museum of Archaeology and Ethnology, 2019).
80. Munro, N. D. & Grosman, L. Early evidence (ca. 12,000 B.P.) for feasting at a burial cave in Israel. *Proc. Natl Acad. Sci. USA* **107**, 15362–15366 (2010).
81. Pettitt, P. *The Palaeolithic Origins of Human Burial* (Routledge, 2011).
82. Garrod, D. A. E. *Les rites funéraires des hommes fossils du Mont-Carmel*, 168–183 (Mélanges Pittard, 1957).
83. Ronen, A. in *African Genesis: Perspectives on Hominin Evolution* (eds Gallagher, A. & Reynolds, S. C.) 554–570 (Cambridge Univ. Press, 2012); <https://doi.org/10.1017/CBO9781139096164.032>
84. Hovers, E., Rak, Y., Lavi, R. & Kimbel, W. H. Hominid remains from Amud Cave in the context of the Levantine Middle Paleolithic. *Paléorient* **21**, 47–61 (1995).
85. Bar-Yosef, O. et al. The excavations in Kebara Cave, Mt. Carmel. *Curr. Anthropol.* **33**, 497–550 (1992).
86. Martínón-Torres, M. et al. Earliest known human burial in Africa. *Nature* **593**, 95–100 (2021).
87. Maureille, B. in *The Routledge Handbook of Archaeothanatology: Bioarchaeology of Mortuary Behaviour* (eds Knüsel, C. J. & Schotsmans, E. M. J.) Ch. 8 (Routledge Handbooks Online, 2022); <https://doi.org/10.4324/9781351030625-11>
88. Suzuki, H. & Takai, F. *The Amud Man and His Cave Site* (Academic Press of Japan, 1970).
89. Bar-Yosef, O. & Vandermeersch, B. *Le Squelette Moustérien de Kébara 2* (Editions du Centre National de la Recherche Scientifique, 1991).

90. Akazawa, T. et al. in *Neanderthal Burials: Excavations of the Dederiyeh Cave, Afrin, Syria* (eds Akazawa, T. & Muhesen, S.) 75–90 (International Research Center for Japanese Studies, 2002).
91. Tillier, A.-M., Arensburg, B., Belfer-Cohen, A. & Vandermeersch, B. Early hominid remains from Hayonim Cave (Israel) in the context of the Late Middle and Upper Pleistocene record from the Near East. *Paléorient* **37**, 47–63 (2011).
92. Hershkovitz, I. et al. Levantine cranium from Manot Cave (Israel) foreshadows the first European modern humans. *Nature* **520**, 216–219 (2015).
93. Hershkovitz, I. et al. The earliest modern humans outside Africa. *Science* **359**, 456–459 (2018).
94. Been, E. et al. The first Neanderthal remains from an open-air Middle Palaeolithic site in the Levant. *Sci. Rep.* **7**, 2958 (2017).
95. May, H. et al. Response to comment on ‘A Middle Pleistocene Homo from Nesher Ramla, Israel’. *Science* **374**, eabl5789 (2021).
96. Valladas, H. et al. Thermoluminescence dating of Mousterian ‘Proto-Cro-Magnon’ remains from Israel and the origin of modern man. *Nature* **331**, 614–616 (1988).
97. Bar-Yosef, O. & Callander, J. The woman from Tabun: Garrod’s doubts in historical perspective. *J. Hum. Evol.* **37**, 879–885 (1999).
98. Stringer, C. New perspectives on the Neanderthals. *Evol. Anthropol.* **11**, 58–59 (2002).
99. Mercier, N. & Valladas, H. Reassessment of TL age estimates of burnt flints from the Paleolithic site of Tabun Cave, Israel. *J. Hum. Evol.* **45**, 401–409 (2003).
100. Tillier, A.-M. The Tabun C1 skeleton: a Levantine Neanderthal? *Mitekufat Haeven*. **35**, 439–450 (2005).
101. Grün, R. & Stringer, C. Direct dating of human fossils and the ever-changing story of human evolution. *Quat. Sci. Rev.* **322**, 108379 (2023).
102. Stringer, C. The origin and evolution of *Homo sapiens*. *Phil. Trans. R. Soc. B* **371**, 20150237 (2016).
103. Garrod, D. The Middle Palaeolithic of the Near East and the problem of Mount Carmel man. *J. R. Anthropol. Inst.* **92**, 232–259 (1962).
104. Brose, D. S. & Wolpoff, M. H. Early Upper Paleolithic man and Late Middle Paleolithic tools. *Am. Anthropol.* **73**, 1156–1194 (1971).
105. Ackermann, R. R., Mackay, A. & Arnold, M. L. The hybrid origin of ‘modern’ humans. *Evol. Biol.* **43**, 1–11 (2016).
106. Kramer, A., Crummett, T. L. & Wolpoff, M. H. Out of Africa and into the Levant: replacement or admixture in western Asia? *Quat. Int.* **75**, 51–63 (2001).
107. Smith, F. H., Janković, I. & Karvanić, I. The assimilation model, modern human origins in Europe, and the extinction of Neandertals. *Quat. Int.* **137**, 7–19 (2005).
108. Hovers, E. in *Neandertals and Moderns Meet* (ed. Conard, N.) 65–85 (Kerns Verlag, 2006).
109. Hublin, J.-J. in *Neandertals and Modern Humans in Western Asia* (eds Akazawa, T. et al.) 295–310 (Springer US, 1998); https://doi.org/10.1007/0-306-47153-1_18
110. Arensburg, B. & Belfer-Cohen, A. in *Neandertals and Modern Humans in Western Asia* (eds Akazawa, T. et al.) 311–322 (Springer US, 1998); https://doi.org/10.1007/0-306-47153-1_19
111. Coutinho-Nogueira, D., Coqueugniot, H., Santos, F. & Tillier, A. The bony labyrinth of Qafzeh 25 *Homo sapiens* from Israel. *Archaeol. Anthropol. Sci.* **13**, 151 (2021).
112. Hershkovitz, I. in *Un Bouquet d’Ancêtres* (eds Coppens, Y. & Viallet, A.) 329–347 (CNRS, 2021).
113. Prévost, M., Groman-Yaroslavski, I., Crater Gershtein, K. M., Tejero, J.-M. & Zaidner, Y. Early evidence for symbolic behavior in the Levantine Middle Paleolithic: a 120 ka old engraved aurochs bone shaft from the open-air site of Nesher Ramla, Israel. *Quat. Int.* **624**, 80–93 (2022).
114. Hovers, E., Vandermeersch, B. & Bar-Yosef, O. A Middle Palaeolithic engraved artefact from Qafzeh Cave, Israel. *Rock Art Res.* **14**, 79–87 (1997).
115. Li, L., Comi, T. J., Bierman, R. F. & Akey, J. M. Recurrent gene flow between Neanderthals and modern humans over the past 200,000 years. *Science* **385**, eadi1768 (2024).
116. Weiner, S. *Microarchaeology: Beyond the Visible Archaeological Record* (Cambridge Univ. Press, 2010).
117. Katz, O. et al. Rapid phytolith extraction for analysis of phytolith concentrations and assemblages during an excavation: an application at Tell es-Safi/Gath, Israel. *J. Archaeol. Sci.* **37**, 1557–1563 (2010).
118. Gur-Arieh, S., Mintz, E., Boaretto, E. & Shahack-Gross, R. An ethnoarchaeological study of cooking installations in rural Uzbekistan: development of a new method for identification of fuel sources. *J. Archaeol. Sci.* **40**, 4331–4347 (2013).
119. Stiner, M. C., Kuhn, S. L., Weiner, S. & Bar-Yosef, O. Differential burning, recrystallization, and fragmentation of archaeological bone. *J. Archaeol. Sci.* **22**, 223–237 (1995).
120. Crouvi, O., Amit, R., Enzel, Y., Porat, N. & Sandler, A. Sand dunes as a major proximal dust source for late Pleistocene loess in the Negev Desert, Israel. *Quat. Res.* **70**, 275–282 (2008).
121. Aitken, M. J. Thermoluminescence dating: past progress and future trends. *Nucl. Tracks Radiat. Meas.* **10**, 3–6 (1985).
122. Kreutzer, S. et al. Environmental dose rate determination using a passive dosimeter: techniques and workflow for α -Al₂O₃:C chips. *Geochronometria* **45**, 56–67 (2018).
123. Kreutzer, S., Tribolo, C., Martin, L. & Mercier, N. Dose-rate estimation using α -Al₂O₃:C chips: aftermath. *Anc. TL* **38**, 1–10 (2020).
124. Prescott, J. R. & Hutton, J. T. Cosmic ray contributions to dose rates for luminescence and ESR dating: large depths and long-term time variations. *Radiat. Meas.* **23**, 497–500 (1994).
125. Valladas, H. Thermoluminescence dating of flint. *Quat. Sci. Rev.* **11**, 1–5 (1992).
126. Guérin, G. & Lefèvre, J.-C. A low cost TL–OSL reader dedicated to high temperature studies. *Measurement* **49**, 26–33 (2014).
127. Aitken, M. J. *Introduction to Optical Dating: The Dating of Quaternary Sediments by the Use of Photon-Stimulated Luminescence* (Oxford Univ. Press, 1998).
128. Nambi, K. S. V. & Aitken, M. J. Annual dose conversion factors for TL and ESR dating. *Archaeometry* **28**, 202–205 (1986).
129. Galbraith, R. F. & Roberts, R. G. Statistical aspects of equivalent dose and error calculation and display in OSL dating: an overview and some recommendations. *Quat. Geochronol.* **11**, 1–27 (2012).
130. Abràmoff, M. D., Magalhães, P. J. & Ram, S. J. Image processing with Image. *J. Biophotonics Int.* **11**, 36–42 (2004).
131. Blockley, S. P. E. et al. A new and less destructive laboratory procedure for the physical separation of distal glass tephra shards from sediments. *Quat. Sci. Rev.* **24**, 1952–1960 (2005).
132. Hayward, C. High spatial resolution electron probe microanalysis of tephra and melt inclusions without beam-induced chemical modification. *Holocene* **22**, 119–125 (2012).
133. Bordes, F. *Typologie du Paléolithique Ancien et Moyen* (Imprimeries Delmas, 1961).
134. Keeley, L. H. *Experimental Determination of Stone Tool Uses: A Microwave Analysis* (Univ. Chicago Press, 1980).
135. Vaughan, P. C. *Use-Wear Analysis of Flaked Stone Tools* (Univ. Arizona Press, 1985).
136. Rots, V. *Prehension and Hafting Traces on Flint Tools: A Methodology* (Leuven Univ. Press, 2010).
137. Stockmarr, J. Tablets with spores used in absolute pollen analysis. *Pollen Spores* **13**, 615–621 (1971).
138. Reille, M. *Pollen et Spores d’Europe et d’Afrique du Nord, Supplément 1* (Laboratoire de Botanique Historique et Palynologie, 1995).

139. Reille, M. *Pollen et Spores d'Europe et d'Afrique du Nord, Supplément 2* (Laboratoire de Botanique Historique et Palynologie, 1998).
140. Reille, M. *Pollen et Spores d'Europe et d'Afrique du Nord* (Laboratoire de Botanique Historique et Palynologie, 1999).
141. Beug, H.-J. *Leitfaden der Pollenbestimmung für Mitteleuropa und angrenzende Gebiete* (G. Fischer, 2004).
142. Valladas, H. & Valladas, G. Effet de l'irradiation alpha sur des grains de quartz. *PACT* **6**, 171–178 (1982).
143. Guérin, G., Mercier, N. & Adamiec, G. Dose-rate conversion factors: update. *Anc. TL* **29**, 5–8 (2011).

Acknowledgements

This work was supported by the Israel Science Foundation (grant numbers 2229/23 and 1936/18 to Y.Z., and 1458/19 and 1084/23 to I.H.), the Dan David Foundation (to I.H. and Y.Z.), the Research Authority at the Hebrew University of Jerusalem (to Y.Z.), the Leakey Foundation to (Y.Z.), the National Geographic Society (grant numbers NGS-72344R-20 to Y.Z. and NGS-51135R-18 to I.H.), the Gerda Henkel Foundation (to I.H.), the Wenner-Gren Foundation (to I.H. and Y.Z.) and the Irene Levi Sala Care Archaeological Foundation (to Y.Z.). The funders had no role in study design, data collection and analysis, decision to publish or preparation of the manuscript. We thank the Israel Nature and Parks Authority for their continuous support during the fieldwork at Tinsmet Cave. We thank the National Natural History Collections of the Hebrew University of Jerusalem for providing comparative material for the study of micromammals. We thank I. Zohar for assisting in the preparation and editing of some of the figures, and D. L. Huber for editing the manuscript. We thank S. Alon for preparing the original maps of the cave. We thank all the students and volunteers who excavated at Tinsmet Cave between 2016 and 2023.

Author contributions

Y.Z., M.P. and I.H. conceived and designed the research and led the fieldwork. Y.Z. and I.H. obtained the main funding grants. The lithic assemblage was analysed and interpreted by M.P., Y.Z. and S.B.-H. A.P. conducted the use-wear analyses of the lithic sample. R.Y. coordinated the analysis of the faunal record. R.Y. and S.L. studied the faunal remains. L.W. conducted the analyses of the micromammals. A.F. conducted the geomorphological study. D.G.-S. and S.I. conducted the study of ochre. N.P. conducted the OSL study. N.M. coordinated the TL dating. N.M., G.G., G.B., C.T. and H.V. conducted the TL analyses. A.G. and C.P. conducted the U-series analyses and produced the associated material. R.S.-G., P.G., A.V.P. and C.N. performed the geoarchaeological study. D.W., R.T. and S. Blockley conducted the

cryptotephra analyses. O.C. conducted the sedimentological analysis. D.L. conducted the pollen analysis. C.Z. and O.V. collected data during the fieldwork. I.H., H.M., R.S. and S. Borgel studied the anthropological remains. All authors drafted and revised the work.

Competing interests

The authors declare no competing interests.

Additional information

Extended data is available for this paper at

<https://doi.org/10.1038/s41562-025-02110-y>.

Supplementary information The online version contains supplementary material available at

<https://doi.org/10.1038/s41562-025-02110-y>.

Correspondence and requests for materials should be addressed to Yossi Zaidner.

Peer review information *Nature Human Behaviour* thanks the anonymous reviewers for their contribution to the peer review of this work. Peer reviewer reports are available.

Reprints and permissions information is available at

www.nature.com/reprints.

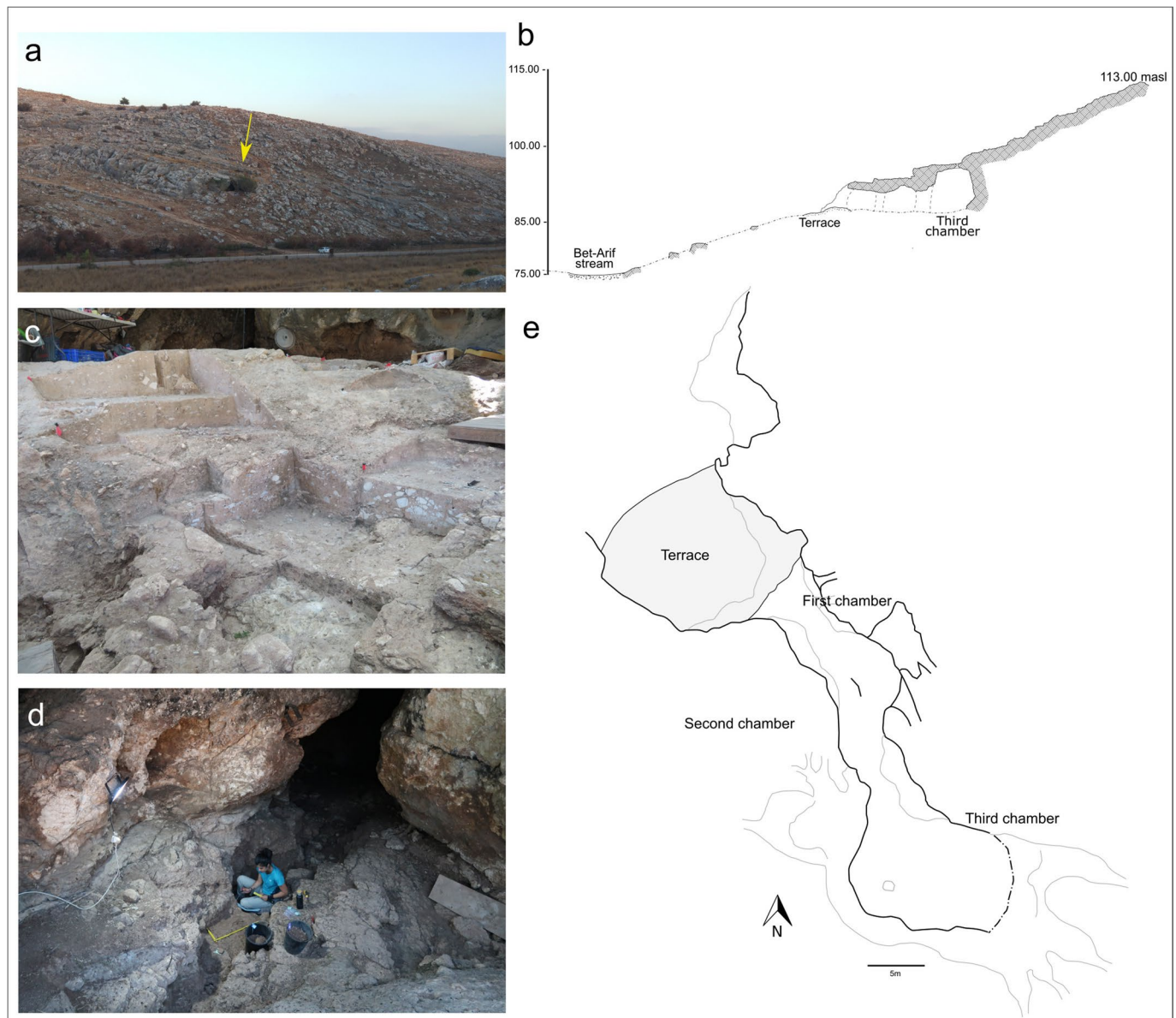
Publisher's note Springer Nature remains neutral with regard to jurisdictional claims in published maps and institutional affiliations.

Open Access This article is licensed under a Creative Commons Attribution-NonCommercial-NoDerivatives 4.0 International License, which permits any non-commercial use, sharing, distribution and reproduction in any medium or format, as long as you give appropriate credit to the original author(s) and the source, provide a link to the Creative Commons licence, and indicate if you modified the licensed material. You do not have permission under this licence to share adapted material derived from this article or parts of it. The images or other third party material in this article are included in the article's Creative Commons licence, unless indicated otherwise in a credit line to the material. If material is not included in the article's Creative Commons licence and your intended use is not permitted by statutory regulation or exceeds the permitted use, you will need to obtain permission directly from the copyright holder. To view a copy of this licence, visit <http://creativecommons.org/licenses/by-nc-nd/4.0/>.

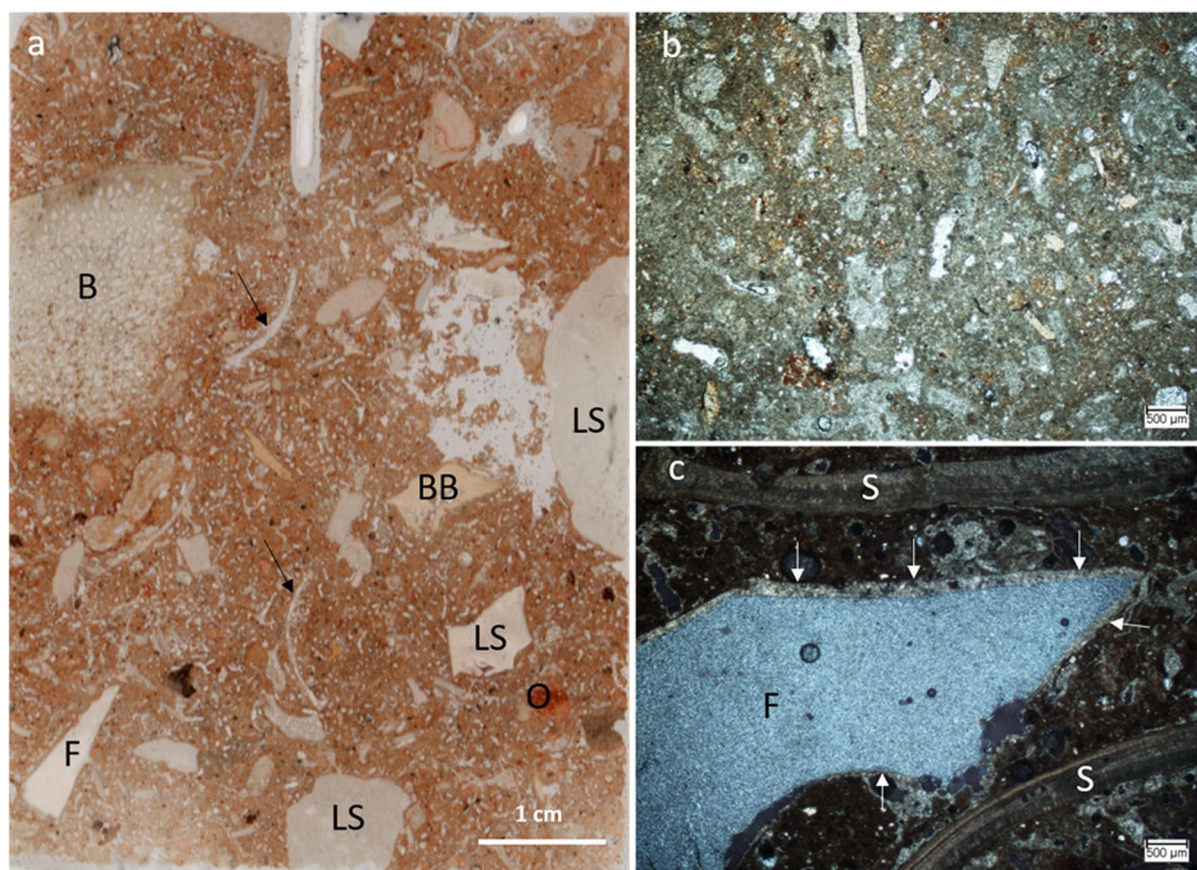
© The Author(s) 2025

¹Institute of Archaeology, Hebrew University, Jerusalem, Israel. ²Department of Maritime Civilizations, Department of Archaeological Sciences, School of Archaeology and Maritime Cultures, Recanati Institute of Maritime Studies, University of Haifa, Haifa, Israel. ³Israel Antiquities Authority, Jerusalem, Israel. ⁴Zinman Institute of Archaeology and School of Archaeology and Maritime Cultures, University of Haifa, Haifa, Israel. ⁵Geological Survey of Israel, Jerusalem, Israel. ⁶Laboratoire des Sciences du Climat et de l'Environnement, LSCE/IPSL, UMR CEA-CNRS-UVSQ 8212 CEA Saclay, Gif sur Yvette Cedex, France. ⁷Archéosciences Bordeaux, UMR 6034 CNRS-Université Bordeaux Montaigne, Pessac Cedex, France. ⁸Université de Pau et des Pays de l'Adour, E2S UPPA, CNRS, IPREM, Pau Cedex, France. ⁹Department of Geography, Royal Holloway, University of London, Egham, UK. ¹⁰Institute of Earth Sciences, Hebrew University of Jerusalem, Jerusalem, Israel. ¹¹Institute of Evolutionary Medicine, University of Zurich, Zurich, Switzerland. ¹²Department of Maritime Civilizations, School of Archaeology and Maritime Cultures, University of Haifa, Haifa, Israel. ¹³Dipartimento di Geoscienze, Università di Padova, Padua, Italy. ¹⁴Department of Bible, Archaeology and the Ancient Near East, Ben-Gurion University of the Negev, Beer-Sheva, Israel. ¹⁵Department of Anthropology, University of Connecticut, Storrs, CT, USA. ¹⁶Steinhardt Museum of Natural History and Laboratory of Archaeobotany and Ancient Environments, Institute of Archaeology, Tel Aviv University, Tel Aviv, Israel. ¹⁷Department of Archaeology and Ancient Near Eastern Cultures, Tel Aviv University, Tel Aviv, Israel. ¹⁸Department of Anatomy and Anthropology, Faculty of Medical and Health Sciences, Tel Aviv University, Tel Aviv, Israel. ¹⁹Dan David Center for Human Evolution and Biohistory Research, Faculty of Medical and Health Sciences, Tel Aviv University, Tel Aviv, Israel. ²⁰Department of Oral Biology, Maurice and Gabriela Goldschleger School of Dental Medicine, Faculty of Medical and Health Sciences, Tel Aviv University, Tel Aviv, Israel.

✉ e-mail: yzaidner@mail.huji.ac.il

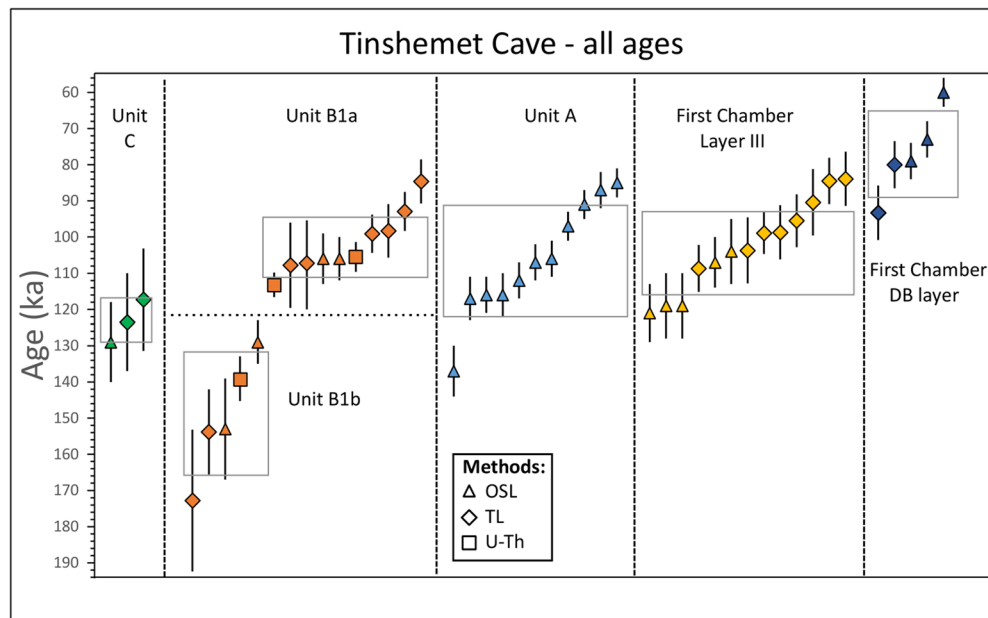


Extended Data Fig. 1 | Tinshemet Cave. **a**, Location of Tinshemet cave, 15 meters above Wadi Bet-Arif. **b**, cross-section of the hill slope with the position of the cave. **c**, View of the terrace. **d**, View of the inside of the first chamber. **e**, Plan of the cave.



Extended Data Fig. 2 | Characteristic micromorphological features of Unit A and Layer III. **a**, Flatbed scan of a thin section representative of Unit A and Layer III deposits, showing the massive light greyish-brown groundmass that contains abundant angular and rounded clasts of limestone (LS), bone (B), burned bone (BB), flint (F), land snail shells (arrows) and ochre (O). **b**, Microphotograph showing the composition of the calcitic clayey groundmass. Note the grey dusty

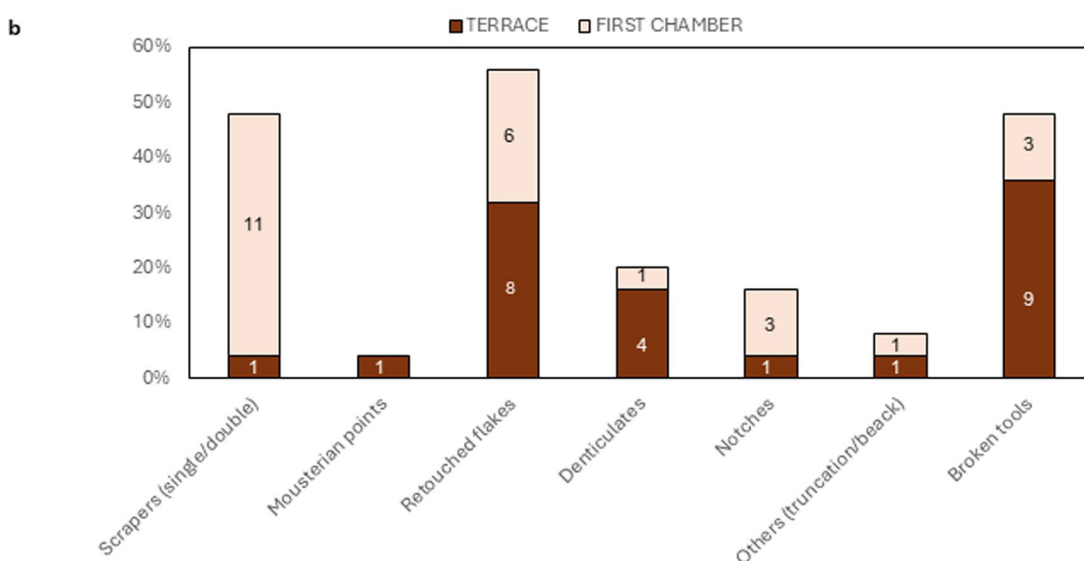
micritic appearance typical of wood ash. The orange-brown patches are reworked Terra Rossa soil aggregates. The porosity is primarily vughs and channels reflecting bioturbation. Pores are commonly infilled by secondary calcite. PPL. **c**, Flint fragment coated by a calcitic (sparite) patina (arrows) reflecting post-depositional calcite dissolution and re-crystallization. Note also two land snail shell fragments (S). XPL.



Extended Data Fig. 3 | Dating of Tinsihemet Cave. Diagram summarizing the dates obtained by the different dating methods. Each data point is a single age (See Extended Data Tables 1–3). Error bars are $\pm 1\sigma$.

a

		TERRACE		FIRST CHAMBER	
	Blanks	n	%	n	%
CORE	Core (varia)	6	0.3%	7	0.9%
	Broken core	10	0.5%	5	0.6%
	Core-on-flake	9	0.5%	5	0.6%
	Hierarchical surface core	5	0.3%	4	0.5%
	Levallois core	22	1.1%	13	1.6%
	Tested nodule	2	0.1%	4	0.5%
DEBITAGE	Entame	8	0.4%	3	0.4%
	Cortical element 25-50%	62	3.1%	44	5.4%
	Cortical element 51-99%	93	4.7%	59	7.3%
	CTE (varia)	43	2.2%	14	1.7%
	Débordant flake	32	1.6%	22	2.7%
	Pseudo-Levallois flake/point	33	1.7%	9	1.1%
	Striking platform preparation flake	6	0.3%	0	0.0%
	Naturally backed knives	13	0.7%	12	1.5%
	Flake	572	29.0%	160	19.8%
	Proximal flake	214	10.9%	39	4.8%
	Levallois flake	127	6.4%	82	10.1%
	Levallois point	2	0.1%	7	0.9%
	Levallois blade	2	0.1%	0	0.0%
	Kombewa flake	23	1.2%	7	0.9%
	Blade	26	1.3%	16	2.0%
	Nahr Ibrahim pieces	1	0.1%	2	0.2%
	Flake from retouch	3	0.2%	0	0.0%
	Fragment	582	29.5%	289	35.7%
	Chunk	51	2.6%	0	0.0%
	Potlid	24	1.2%	6	0.7%
	TOTAL	1971		809	



Extended Data Fig. 4 | Lithic assemblages (technology and typology) at Tinshemet Cave. a. General breakdown of the studied lithic assemblages. **b.** Retouched tools categories frequency per areas.

Extended Data Table 1 | Dosimetric data and TL age estimates

Sample n°	Unit/Layer	Square	U (ppm)	Th (ppm)	K (%)	S-alpha	alpha	beta	Internal	+ - $\mu\text{Gy/a}$	Gamma	Cosmic	External	+ -	Annual	+ -	Paleodose (Gy)	+ -	Age (ka)	+ -
TIN-1	DB	AO 18	0.436	0.072	0.026	16.2	123.1	86.5	209.7	16	502	100	602	59.4	811.7	61.5	75.7	2	93	7
TIN-22	DB	AO 18	0.942	0.057	0.023	17.6	280.6	157.1	437.8	36.9	502	100	602	70.2	1039.8	79.3	83.2	2.2	80	6
TIN-14-1	III	AN 18	3.076	0.028	0.024	18.4	943.8	468.1	1412	125.7	502	100	602	153.1	2014	198.1	182	4.5	90	9
TIN-4	III	AN 21	0.699	0.049	0.02	10.8	128.1	119.1	247.3	18	361	100	461	34.5	708.3	39	77	1.9	109	7
TIN-13	III	AM 21	1.611	0.012	0.04	16.4	440.3	266.9	707.3	59.4	360	100	460	64	1167.3	87.3	121	5.6	104	9
TIN-9	III	AM 20	0.558	0.067	0.028	15.3	146.9	105.2	252.2	19.4	409	100	509	50.9	761.2	54.5	72.7	1.9	95	7
TIN-20	III	AM 20	0.987	0.052	0.042	12.3	205	178.3	383.4	28.4	409	100	509	56.9	892.4	63.6	88.1	2.2	99	7
TIN-23	III	AM 20	0.315	0.106	0.047	13.4	77.1	85.9	163	10.1	409	100	509	47.8	672	48.9	56.8	1.2	85	6
TIN-11	III	AO 20	1.173	0.013	0.017	24.2	473.6	184.9	658.5	62	361	100	461	75	1119.5	97.3	93.9	2	84	8
TIN-15	III	AO 19	0.284	0.064	0.024	13	65.4	61.9	127.4	8.7	457	100	557	35	684.4	36.1	67.7	1.7	99	6
TIN-16	B1a	AE 23	3.824	0.021	0.02	19.8	1261.3	573.5	1834.9	167.3	398.9	140	538.9	190.2	2373.8	253.3	256	6.6	108	12
TIN-18-1	B1a	AD 23	2.566	0.014	0.02	25.7	1098.6	390	1488.6	143.5	398.9	140	538.9	163	2027.5	217.2	217.4	5.2	107	12
TIN-19	B1a	AD 23	0.446	0.126	0.024	14.9	119.6	87.7	207.3	15.2	398.9	140	538.9	34.2	746.3	37.5	69.3	2	93	5
TIN-21	B1a	AE 23	1.318	0.03	0.012	16.2	357.4	202.5	560	47.9	398.9	140	538.9	61.4	1098.9	77.9	108	2.8	98	7
TIN-24	B1a	AD 23	0.336	0.139	0.055	15	93.9	96.6	190.6	12	398.9	140	538.9	33.8	729.5	35.9	72.3	1.5	99	5
TIN-667	B1a	AF 23b	0.604	0.742	0.046	14	191.2	145	336.2	23.2	441.9	140	581.9	56.2	918.2	60.8	77.7	2.1	85	6
TIN-361	B1b	AF 24d	2.088	0.501	0.021	23.3	866	334.9	1200.9	118.7	441.9	140	581.9	150.5	1782.9	191.7	308.1	11.1	173	20
TIN-160	B1b	AF 24d	0.372	0.816	0.039	24.9	253	108.2	361.3	26.7	441.9	140	581.9	59.8	943.2	65.5	145.1	4.7	154	12
TIN-3	C	AE 25	7.465	0.036	0.013	17.9	2225.6	1098.9	3324.5	235.5	397	140	537	338.7	3861.6	412.5	477	11.8	124	14
TIN-5	C	AE 25	5.833	0.009	0.014	20.5	1989.7	861.2	2851	263.7	397	140	537	294.6	3388	395.4	397.5	11.4	117	14

S-alpha represents the relative efficiency of alpha particles (from a calibrated ^{241}Am source) compared to beta rays (from a calibrated ^{90}Sr source) at inducing a TL signal¹⁴². Dose-rate conversion factors of Guérin et al.¹⁴³ were used to calculate the ages. A systematic error of 10% was assigned to the U, Th and K contents and a value of 3% for the beta source calibration. In bold are the average date for each sample.

Extended Data Table 2 | OSL laboratory data and ages for all samples, arranged by layer

Lab code	Unit/Layer	Depth (m)	K (%)	U (ppm)	Th (ppm)	Alpha (μGy/a)	Beta (μGy/a)	Gamma (μGy/a)	Cosmic (μGy/a)	Dose rate (μGy/a)	N	OD (%)	De (Gy)	Age (ka)
TNS-16	A1	0.7	0.31	1.4	1.5	5	392	273	196	866±29	19/19	9	92±3	106±5
TNS-21	A1	0.7	0.27	1.4	1.2	4	360	252	196	812±29	18/18	7	87±2	107±5
TNS-22	A1	0.7	0.28	1.6	0.7	5	375	249	196	824±28	18/18	9	96±3	116±6
Average	A1													110±6
TNS-17	A2	0.85	0.38	1.7	1.7	6	480	331	189	1006±35	19/19	6	91±2	91±4
TNS-18	A2	0.85	0.34	1.6	1.5	5	438	304	189	936±40	18/19	12	79±2	85±4
TNS-19	A2	0.75	0.44	1.6	1.5	5	493	317	193	1008±41	17/18	24	88±3	87±5
Average	A2													88±3
TNS-14	A3	0.7	0.29	1.3	1.6	4	367	260	196	828±30	20/20	9	93±3	112±6
TNS-15	A3	0.8	0.24	1.8	1.2	6	394	290	190	880±30	20/20	8	86±2	97±4
TNS-23	A3	0.85	0.23	1.0	1.4	4	290	209	189	691±23	18/18	13	95±3	137±7
Average	A3													115±17
TNS-20	A4	0.75	0.25	1.4	1.4	5	348	252	193	979±30	18/18	14	92±3	116±6
TNS-24	A4	0.9	0.27	1.4	1.7	5	368	269	187	829±34	17/17	12	97±3	117±6
Average	A4													116±2
TNS-5	B1a	0.7	0.35	2.3	2.9	8	599	479	196	1242±63	19/19	14	131±5	106±7
TNS-1	B1b	0.9	0.30	1.2	1.3	4	355	341	187	888±77	19/19	13	136±5	153±14
TNS-6	B1b	0.9	0.35	3.4	2.1	10	670	513	187	1381±66	18/18	13	146±5	106±6
TNS-7	B1b	0.9	0.32	2.2	1.7	7	493	361	187	1049±37	20/20	8	135±4	129±6
Average	B													123±19
TNS-2	C	0.95	0.34	2.1	1.2	6	487	341	186	1021±82	19/19	11	132±4	129±11
TNS-11	DB	3.5	1.37	2.0	5.7	9	1158	708	137	2012±94	19/19	17	147±6	73±5
TNS-12	DB	3.5	1.37	2.1	4.4	8	1146	667	137	1958±89	19/20	24	155±7	79±5
TNS-13	DB	3.5	1.38	2.4	7.5	11	1249	824	137	2220±98	16/17	24	134±7	60±4
Average	DB													71±8
TNS-3	FC	3.0	1.01	2.2	3.8	8	923	307	145	1383±84	18/18	25	144±9	104±9
TNS-4	FC	3.5	0.99	2.2	3.9	8	919	578	137	1642±83	19/19	24	195±11	119±9
TNS-8	FC	3.5	0.84	1.8	2.6	6	755	453	137	1351±60	19/19	18	164±7	121±8
TNS-9	FC	3.5	0.59	2.1	1.7	6	619	392	137	1154±51	19/19	25	138±8	119±9
TNS-10	FC	3.5	0.54	1.9	1.5	6	568	357	137	1068±53	19/20	17	112±5	107±7
Average	FC													114±8

Layers A-C are on the terrace; DB – dark brown layer in the first chamber; FC – first chamber, light brown layer. Grain size for all samples is 75-125 μm. Burial depth for samples from the terrace includes additional 0.6 m of topsoil that was removed during excavations. Moisture contents estimated at 10±3% and 15±4% for samples from terrace and chamber, respectively. Gamma dose rate was calculated from radioelement contents or averaged with dosimeters where available. For most samples, chemical analyses were carried out on several (2-5) subsamples and the values averaged. Errors on radioelement concentrations are 7-10% of the measured values. In bold are the average date for each layer. N - The number of aliquots used for calculating the De out of those measured (outliers removed). OD - overdispersion, a measure of the scatter within the sample beyond that expected from instrumental noise.

Extended Data Table 3 | U/Th ages of snail shells from Tinshemet Cave

Samples	Layer	$(^{230}\text{Th}/^{232}\text{Th})$		$(^{230}\text{Th}/^{234}\text{U})$		$(^{234}\text{U}/^{238}\text{U})$		Age (ka)
<i>Tm19SSh1</i>	B1a	3325	54	0.661	0.006	1.199	0.005	113.3 +3.3/-3.5
<i>Tm19SSh2</i>	B1a	559	65	0.992	0.009	1.380	0.006	272 +728/-17
<i>Tm19SSh6</i>	B1b	678	40	0.741	0.009	1.201	0.006	138.9 +6.4/-6.0
<i>Tm19SSh8</i>	B1b	627	36	0.639	0.008	1.294	0.007	105.5 ±4.1

Activity ratios and U/Th ages of snail shells.

Extended Data Table 4 | Breakdown of the Levallois assemblages at Tinshemet Cave

Breakdown of the Levallois assemblages	TERRACE		FIRST CHAMBER	
	n	%	n	%
Levallois core (total)	22	10%	13	10%
broken	3	14%	0	0%
centripetal	16	73%	13	100%
bidirectional	2	9%	0	0%
unknown	1	5%	0	0%
Levallois flake (total)	127	57%	82	62%
centripetal	48	61%	44	75%
unidirectional	19	24%	5	8%
bidirectional	8	10%	9	15%
convergent	4	5%	1	2%
Unknown (broken, patinated, burnt)	48		23	
Levallois point	2	1%	7	5%
Levallois blade	2	1%	0	0%
Pseudo Levallois flake/point	33	15%	9	7%
<i>Débordant</i> flake	32	14%	22	17%
Striking platform preparation' flake	6	3%	0	0%
	224		133	

Representation of the Levallois reduction systems according to their technological characteristics.

Extended Data Table 5 | Vertebrates' taxonomic composition at Tinshemet Cave

Taxonomic group	First Chamber Layer III	First Chamber DB layer	Terrace	Indet.	Total NISP	% NISP
<i>Gazella gazella</i>	7	17	14	8	46	24.08
<i>Capra</i> sp.		1	3	3	7	3.66
<i>Dama mesopotamica</i>	7	12	12	3	34	17.80
<i>Cervus elaphus</i>	1			2	3	1.57
<i>Sus scrofa</i>	1		2	1	4	2.09
<i>Equus</i> spp.	4	3	14	6	27	14.14
<i>Bos primigenius</i>	11	14	14	8	47	24.61
Rhinocerotidae			1		1	0.52
<i>Hystrix</i> sp.	1	2			3	1.57
Small carnivore	1				1	0.52
Hyena/Crocuta		1			1	0.52
Large carnivore		1			1	0.52
Aves	3	2			5	2.62
<i>Testudo graeca</i>	1	1			2	1.05
Snake and lizard	3	2	4		9	4.71
Total	40	56	64	31	191	100%

Taxonomic composition of Tinshemet animal bone assemblage (Number of Identified Specimens, NISP), according to depositional contexts.

Reporting Summary

Nature Portfolio wishes to improve the reproducibility of the work that we publish. This form provides structure for consistency and transparency in reporting. For further information on Nature Portfolio policies, see our [Editorial Policies](#) and the [Editorial Policy Checklist](#).

Statistics

For all statistical analyses, confirm that the following items are present in the figure legend, table legend, main text, or Methods section.

n/a Confirmed

- | | | |
|-------------------------------------|-------------------------------------|--|
| <input type="checkbox"/> | <input checked="" type="checkbox"/> | The exact sample size (n) for each experimental group/condition, given as a discrete number and unit of measurement |
| <input type="checkbox"/> | <input checked="" type="checkbox"/> | A statement on whether measurements were taken from distinct samples or whether the same sample was measured repeatedly |
| <input checked="" type="checkbox"/> | <input type="checkbox"/> | The statistical test(s) used AND whether they are one- or two-sided
<i>Only common tests should be described solely by name; describe more complex techniques in the Methods section.</i> |
| <input checked="" type="checkbox"/> | <input type="checkbox"/> | A description of all covariates tested |
| <input checked="" type="checkbox"/> | <input type="checkbox"/> | A description of any assumptions or corrections, such as tests of normality and adjustment for multiple comparisons |
| <input type="checkbox"/> | <input checked="" type="checkbox"/> | A full description of the statistical parameters including central tendency (e.g. means) or other basic estimates (e.g. regression coefficient) AND variation (e.g. standard deviation) or associated estimates of uncertainty (e.g. confidence intervals) |
| <input type="checkbox"/> | <input checked="" type="checkbox"/> | For null hypothesis testing, the test statistic (e.g. F , t , r) with confidence intervals, effect sizes, degrees of freedom and P value noted
<i>Give P values as exact values whenever suitable.</i> |
| <input checked="" type="checkbox"/> | <input type="checkbox"/> | For Bayesian analysis, information on the choice of priors and Markov chain Monte Carlo settings |
| <input checked="" type="checkbox"/> | <input type="checkbox"/> | For hierarchical and complex designs, identification of the appropriate level for tests and full reporting of outcomes |
| <input checked="" type="checkbox"/> | <input type="checkbox"/> | Estimates of effect sizes (e.g. Cohen's d , Pearson's r), indicating how they were calculated |

Our web collection on [statistics for biologists](#) contains articles on many of the points above.

Software and code

Policy information about [availability of computer code](#)

Data collection No software was used

Data analysis No software was used

For manuscripts utilizing custom algorithms or software that are central to the research but not yet described in published literature, software must be made available to editors and reviewers. We strongly encourage code deposition in a community repository (e.g. GitHub). See the Nature Portfolio [guidelines for submitting code & software](#) for further information.

Data

Policy information about [availability of data](#)

All manuscripts must include a [data availability statement](#). This statement should provide the following information, where applicable:

- Accession codes, unique identifiers, or web links for publicly available datasets
- A description of any restrictions on data availability
- For clinical datasets or third party data, please ensure that the statement adheres to our [policy](#)

The data is available in the supplementary information and extended data files. The archaeological materials are hosted in the Hebrew University of Jerusalem and in the Haifa University and are accessible upon request

Research involving human participants, their data, or biological material

Policy information about studies with [human participants or human data](#). See also policy information about [sex, gender \(identity/presentation\), and sexual orientation](#) and [race, ethnicity and racism](#).

Reporting on sex and gender n/a

Reporting on race, ethnicity, or other socially relevant groupings n/a

Population characteristics n/a

Recruitment n/a

Ethics oversight n/a

Note that full information on the approval of the study protocol must also be provided in the manuscript.

Field-specific reporting

Please select the one below that is the best fit for your research. If you are not sure, read the appropriate sections before making your selection.

☐ Life sciences

☒ Behavioural & social sciences

☐ Ecological, evolutionary & environmental sciences

For a reference copy of the document with all sections, see [nature.com/documents/nr-reporting-summary-flat.pdf](https://www.nature.com/documents/nr-reporting-summary-flat.pdf)

Behavioural & social sciences study design

All studies must disclose on these points even when the disclosure is negative.

Study description	Study of the lithic technology, ochre type and provenience, zooarchaeological remains and burial practices at the Middle Palaeolithic site of Tinshemet Cave. Mixed methods
Research sample	Stone tools, sediments, ochre and animal bones from the Middle Palaeolithic site of Tinshemet Cave. The sample is representative. All the excavated material from main habitation areas of the site were studied
Sampling strategy	Three major areas of the Tinshemet Cave were sampled. Entire assemblages from the sampled areas were studied. During excavation all the materials larger than 1 mm in length were collected and studied
Data collection	Data was collected during the archaeological excavations at Tinshemet Cave. Excavation tools were used for collection the materials. For the sieving mesh with 1 mm holes was used
Timing	Summer 2016- summer 2023
Data exclusions	No data was excluded from the analyses
Non-participation	No participants were involved in the study
Randomization	Randomization is usually not applied in the studies of archaeological materials

Reporting for specific materials, systems and methods

We require information from authors about some types of materials, experimental systems and methods used in many studies. Here, indicate whether each material, system or method listed is relevant to your study. If you are not sure if a list item applies to your research, read the appropriate section before selecting a response.

Materials & experimental systems

n/a	Involvement in the study
<input checked="" type="checkbox"/>	<input type="checkbox"/> Antibodies
<input checked="" type="checkbox"/>	<input type="checkbox"/> Eukaryotic cell lines
<input type="checkbox"/>	<input checked="" type="checkbox"/> Palaeontology and archaeology
<input checked="" type="checkbox"/>	<input type="checkbox"/> Animals and other organisms
<input checked="" type="checkbox"/>	<input type="checkbox"/> Clinical data
<input checked="" type="checkbox"/>	<input type="checkbox"/> Dual use research of concern
<input checked="" type="checkbox"/>	<input type="checkbox"/> Plants

Methods

n/a	Involvement in the study
<input checked="" type="checkbox"/>	<input type="checkbox"/> ChIP-seq
<input checked="" type="checkbox"/>	<input type="checkbox"/> Flow cytometry
<input checked="" type="checkbox"/>	<input type="checkbox"/> MRI-based neuroimaging

Palaeontology and Archaeology

Specimen provenance	Specimens were excavated from Tinsmet Cave. The excavations permits were provided by Israel Antiquity Authority. Permit number: G-27 /2021
Specimen deposition	The Institute of Archaeology, the Hebrew University of Jerusalem
Dating methods	New TL, OSL and U/Th dates are included in the publication. The scientists that conducted the analyses co-author this paper. The OSL dates were provided by the Geological Survey of Israel. TL dates were provided by Archeosciences Bordeaux, Universite Bordeaux Montaigne, France.
<input checked="" type="checkbox"/> Tick this box to confirm that the raw and calibrated dates are available in the paper or in Supplementary Information.	
Ethics oversight	No ethical approval or guidance were required for this study

Note that full information on the approval of the study protocol must also be provided in the manuscript.

Plants

Seed stocks	n/a
Novel plant genotypes	n/a
Authentication	n/a